AD A091605

ULTRASONIC ATTENUATION IN NORMAL AND
SUPERCONDUCTING INDIUM

Michael P. Conley

Technical Memorandum
File No. TM 80-126
May 22, 1980
Contract No. N00024-79-C-6043

Copy No. _15_

The Pennsylvania State University
Intercollege Research Programs and Facilities
APPLIED RESEARCH LABORATORY
Post Office Box 30
State College, PA 16801

NAVY DEPARTMENT

NAVAL SEA SYSTEMS COMMAND

80 10 31 073

(9) Technical memo. for period ending Aug 89

REPORT DOCUMENTATION PAGE	READ INSTRUCTIONS BEFORE COMPLETING FORM

(14)

ARL/PSU

1. REPORT NUMBER TM-80-126	2. GOVT ACCESSION NO. AD-A091 605	3. RECIPIENT'S CATALOG NUMBER

(6)

4. TITLE (and Subtitle) ULTRASONIC ATTENUATION IN NORMAL AND SUPERCONDUCTING INDIUM	5. TYPE OF REPORT & PERIOD COVERED PhD Thesis, August 1980
	6. PERFORMING ORG. REPORT NUMBER TM 80-126

(10)

7. AUTHOR(s) Michael P. Conley	8. CONTRACT OR GRANT NUMBER(s) (15) N00024-79-C-6043

9. PERFORMING ORGANIZATION NAME AND ADDRESS The Pennsylvania State University Applied Research Laboratory P. O. Box 30, State College, PA 16801	10. PROGRAM ELEMENT, PROJECT, TASK AREA & WORK UNIT NUMBERS (11) 22 May 80
11. CONTROLLING OFFICE NAME AND ADDRESS Naval Sea Systems Command Department of the Navy Washington, DC 20362	(12) 12. REPORT DATE May 22, 1980
	13. NUMBER OF PAGES 106 104 pages & figures
14. MONITORING AGENCY NAME & ADDRESS(If different from Controlling Office)	15. SECURITY CLASS. (of this report) Unclassified, Unlimited
	15a. DECLASSIFICATION/DOWNGRADING SCHEDULE

16. DISTRIBUTION STATEMENT (of this Report)

Approved for public release, distribution unlimited,
per NSSC (Naval Sea Systems Command), 7/2/80

17. DISTRIBUTION STATEMENT (of the abstract entered in Block 20, if different from Report)

18. SUPPLEMENTARY NOTES

19. KEY WORDS (Continue on reverse side if necessary and identify by block number)

ultrasonic, attenuation, indium

20. ABSTRACT (Continue on reverse side if necessary and identify by block number)

The dependence of ultrasonic attenuation on temperature, sonic frequency, propagation direction, and superconducting state has been measured in indium single crystals using low-amplitude longitudinal waves. These measurements and the experimental apparatus with which they have been obtained are described.

These data indicate that, in addition to the usual electronic attenuation described quantitatively by the BCS theory of superconductivity (Bardeen et al, Phys. Rev. 108, 1175), there is an additional source of attenuation. This

20. ABSTRACT (continued)

secondary attenuation is generally attributed to the interaction of sound waves and crystal dislocations within the specimen, a process which has been described most thoroughly by Granato and Lücke (J. Appl. Phys. 27, 583).

A comparison of the measured dislocation attenuations with those predicted by the theory of Granato and Lücke is given. This theory is shown to be inapplicable to the situation of this experiment, i.e., to indium at low temperatures. Earlier works in which similar data appear to substantiate the Granto and Lücke theory of dislocation attenuation are shown to be insufficient tests of that theory.

ABSTRACT

The dependence of ultrasonic attenuation on temperature, sonic frequency, propagation direction,and superconducting state has been measured in indium single crystals using low-amplitude longitudinal waves. These measurements and the experimental apparatus with which they have been obtained are described.

These data indicate that, in addition to the usual electronic attenuation described quantitatively by the BCS theory of super-conductivity (Bardeen et al., Phys. Rev. 108, 1175), there is an additional source of attenuation. This secondary attenuation is generally attributed to the interaction of sound waves and crystal dislocations within the specimen, a process which has been described most thoroughly by Granato and Lücke (J. Appl. Phys. 27, 583).

A comparison of the measured dislocation attenuations with those predicted by the theory of Granato and Lücke is given. This theory is shown to be inapplicable to the situation of this experiment, i.e., to indium at low temperatures. Earlier works in which similar data appear to substantiate the Granato and Lücke theory of dislocation attenuation are shown to be insufficient tests of that theory.

TABLE OF CONTENTS

LIST OF FIGURES

LIST OF FIGURES (cont.)

LIST OF SYMBOLS

A	area swept out by a moving dislocation
a	interatomic distance
α	ultrasonic attenuation
α_d	ultrasonic attenuation due to dislocations
α_{dn}	ultrasonic attenuation due to dislocations, normal state
α_{ds}	ultrasonic attenuation due to dislocations, superconducting state
α_e	ultrasonic attenuation due to electrons
α_{en}	ultrasonic attenuation due to electrons, normal state
α_{es}	ultrasonic attenuation due to electrons, superconducting state
α_m	measured ultrasonic attenuation
α_{mn}	measured ultrasonic attenuation, normal state
α_{ms}	measured ultrasonic attenuation, superconducting state
α_r	residual system ultrasonic attenuation
B	dislocation drag coefficient
$\vec{b}, b$	Burgers vector
B_e	electron component of the dislocation drag
B_p	phonon component of the dislocation drag
B_r	radiation component of the dislocation drag
B_0	dislocation drag constant
$\beta(T)$	BCS attenuation ratio
C	effective dislocation line tension
D	reduced dislocation drag coefficient
d	crystal element dimension

LIST OF SYMBOLS (cont.)

D_0 decrement parameter

Δ dislocation decrement

Δ_ℓ single dislocation loop decrement

δ_n constant

e natural base

$\epsilon(T)$ BCS superconducting energy gap parameter

ϵ crystal strain

ϵ_{el} elastic component of the crystal strain

ϵ_{dis} dislocation component of the crystal strain

ϵ_0 BCS superconducting energy gap parameter at $T = 0$

F force on a dislocation

ϕ constant

G shear modulus

h crystal element dimension

k Boltzman's constant

L average dislocation loop length

$\vec{\ell}, \ell$ dislocation loop length, vector parallel to the dislocation line

Λ dislocation density

λ ultrasonic wavelength

$N(\ell)$ distribution of dislocation loop lengths

n summation index

$\vec{\nu}$ unit vector tangent to the dislocation

Ω reduced ultrasonic frequency

ω ultrasonic angular frequency

LIST OF SYMBOLS (cont.)

ω_0 single loop angular frequency, decrement parameter

ρ mass density, residual system attenuation

σ shear stress, attenuation calibration shift

σ_0 effective shear stress

T temperature

t time, reduced temperature

T_c superconducting transition temperature

T_0 lowest temperature of attenuation measurement

V crystal element volume

$\vec{\nu}$ dislocation velocity

w crystal element dimension

x space coordinate, dislocation displacement

ξ dislocation displacement

y space coordinate

z space coordinate

ACKNOWLEDGMENTS

I. INTRODUCTION

The serious study of ultrasonic attenuation in superconducting materials was initiated by the independent discoveries by Bömmel (1954) and Mackinnon (1955) of a dramatic decrease in sound attenuation which accompanied the transition of their specimens into the superconducting state. Bömmel's original data on a single crystal of lead at 26.5 MHz is shown in Figure 1. This phenomenon was first explained quantitatively by Bardeen, Cooper, and Schrieffer (1957) (hereafter referred to as BCS) in their theory of superconductivity. According to the BCS theory, there appears at the Fermi surface an energy gap $2\epsilon(T)$ which increases in width as the temperature is lowered below the superconducting transition point. Reevaluation of the theory of ultrasonic attenuation in metals (Pippard, 1955) with considerations to this energy gap model has led BCS to the following expression for the ratio of superconducting attenuation to that in the normal state:

$$\frac{\alpha_s(T)}{\alpha_n(T)} = \frac{2}{1 + e^{\epsilon(T)/kT}} \quad . \tag{1.1}$$

This predicted behavior was first verified experimentally by Morse and Bohm (1957) and has since been shown by others to apply remarkably well in many elements, compounds and alloys.

Most superconductors exhibit attenuation characteristics which agree with the BCS prediction described above. However, in some
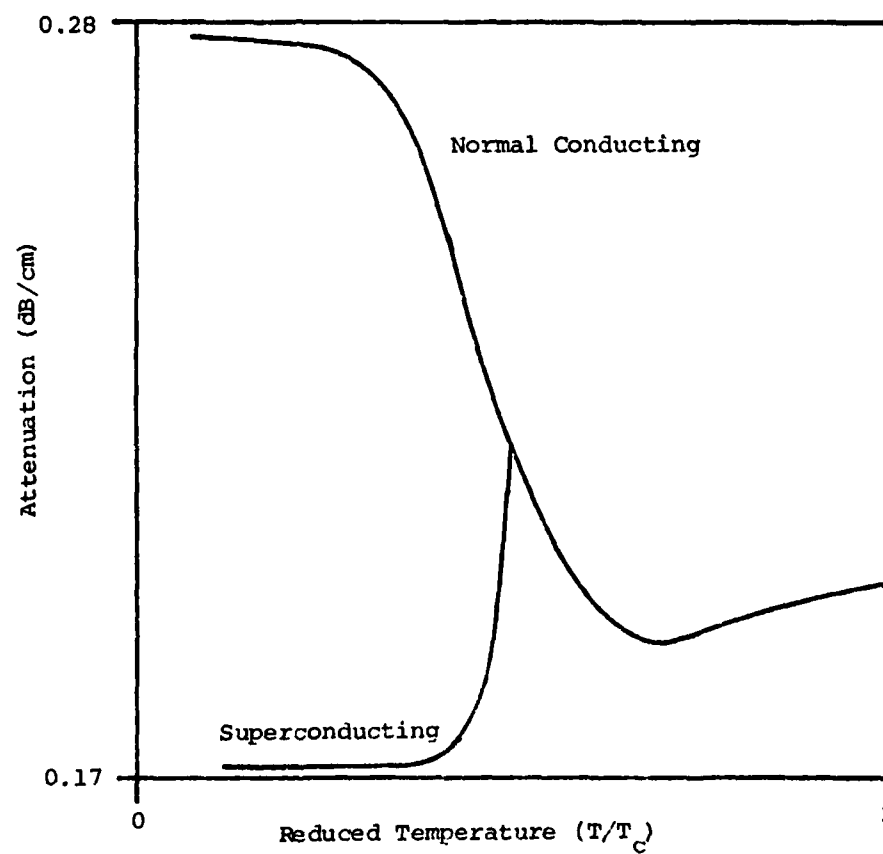
Figure 1. Attenuation of longitudinal waves in superconducting lead as a function of temperature (after Bömmel, 1954).

metals, primarily in high purity single crystals of lead and indium, experiments have disclosed pronounced deviations from the predicted behavior. The work of Love and Shaw (1964), for instance, reveals a case in which the ultrasonic attenuation in the superconducting state is dependent upon the sound amplitude, while in the normal state, it is not. A subsequent study by Tittmann and Bömmel (1966) shows this anomalous behavior to persist even at the lowest amplitudes and that, in this region, the deviations from BCS theory become amplitude independent. Similar data taken by Morse (1959), which shows the nature of the deviation, is plotted in Figure 2. The source of these irregularities has been identified as the interaction of crystal dislocations with the ultrasonic waves. A short review of the evidence for this has been given by Tittmann (1975). Experimental indications that dislocations play a dominant role in this process include the dependence of the amplitude effect on specimen deformation, annealing and purity.

A theory which anticipates the ultrasonic attenuation due to the presence of dislocations has been developed by Granato and Lücke (1956). This work is based on the dislocation-string model of Koehler (1952) which considers a dislocation to have mechanical properties equivalent to those of a taut string. In the low amplitude version of the KGL theory, sound waves in the crystal are expected to drive the dislocation-string into damped oscillations. The motion of the dislocation lags that of the crystal matrix, resulting in a phase difference between stress and strain. This, in turn, results in an

Attenuation Ratio

1

BCS

Data

0

1.0   Temperature (Kelvin)   3.5
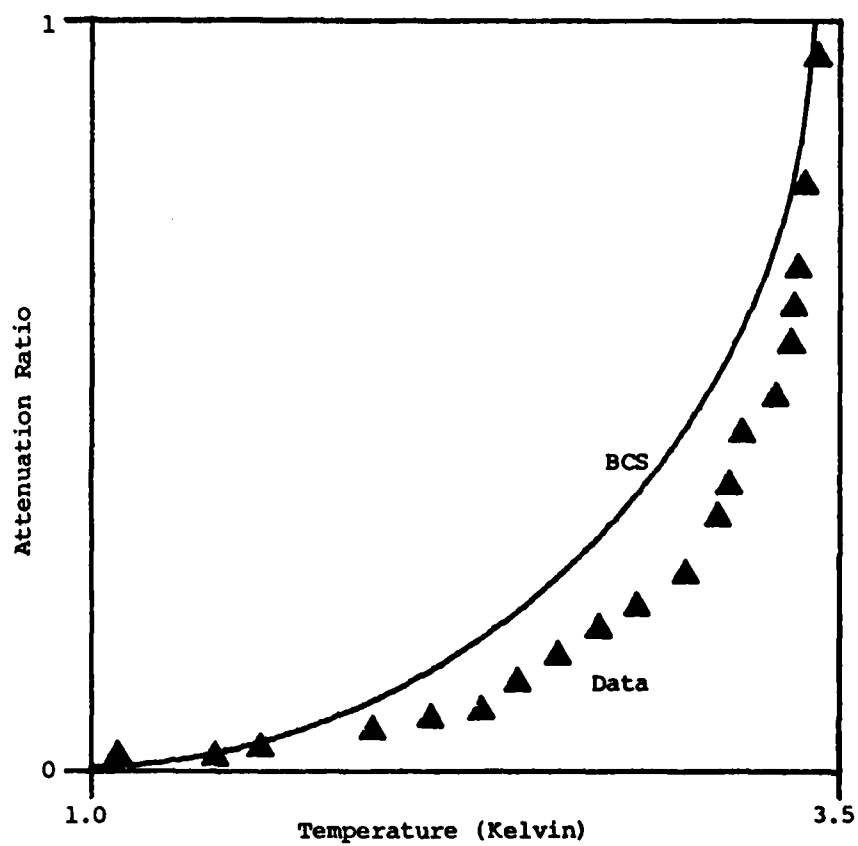
Figure 2. Deviation of measured attenuations from BCS-like
behavior (after Morse, 1959).

attenuation of the sound wave. This theory has found considerable success in describing a variety of dislocation phenomena. The experiments of Thompson and Holmes (1956), who measure the changes of attenuation of pure single crystals of copper under fast neutron irridation, confirm the validity of the theory at low frequencies and room temperature. Merkulov and Yakovlev (1960) have measured the attenuation as a function of frequency in room temperature NaCl deformed 1%, and find good over-all agreement with the theory.

Another apparent verification of the KGL theory is to be found in the work of Mason (1966), who uses a form of the dislocation-string model to explain the anomalous behavior observed in superconductors, as described above. Mason has analyzed low-amplitude attenuation data collected by several investigators and finds that, in each case, the deviations of measured attenuations from those predicted by the BCS relation can be attributed to oscillating dislocation-strings. In the course of this analysis, Mason extracts from the data implied values for certain crystal parameters, such as the density and average length of dislocations within the specimen, which are difficult to obtain by direct measurement. These results may be criticized for the narrow scope of data used in the analysis; in only a single case were attenuations in a particular specimen recorded using more than one frequency of ultrasound and, in that instance, the frequencies varied by a factor of only 1.6.

It is the purpose of this investigation to further study the anomalous behavior of ultrasonic attenuation in superconductors. By

recording single specimen data using as wide a range of ultrasonic frequencies as possible, a most rigorous test of the relevance of the KGL theory to this phenomenon was made. Subsequent to verification that the dislocation-string model properly explained the observed deviations from BCS-like behavior, it was the intent of this research, following the example of Mason, to show the viability of employing ultrasonic attenuation measurements for the nondestructive evaluation of the dislocation character of a superconducting metal. Development of an evaluation procedure has been frustrated by the realization that the interaction of sound waves with dislocations in low temperature indium is not properly described by the KGL theory of dislocation damping. This thesis presents a review of the dislocation-string model of Koehler and the ensuing dislocation attenuation theory of Granato and Lücke. An experimental system by which this theory has been tested is described. Finally, the experimental results which indicate the inapplicability of the KGL theory to low temperature indium will be discussed.

II. THEORY

A. Justification for the Koehler Model

An ideal crystal is constructed by the infinite regular repetition in space of identical structural units. A real crystal differs from this perfect scheme by the defects it contains. Vacancies left by missing atoms, crowding by extra atoms, impurities, and the surface of the crystal itself are examples of the possible defects. The defect of primary concern to this work is a misalignment of atoms within the crystal. An example of this type of fault is illustrated in the two-dimensional crystal of Figure 3. Here, the inconsistency of the atomic pattern in the neighborhood of the point D is termed a dislocation. At a sufficient distance from the dislocation, at A, for example, the crystal is only slightly distorted and retains an unmistakable local correspondence to the ideal atomic lattice. Regions of the crystal where such an atom-by-atom correspondence is unmistakable are labeled regions of good crystal; otherwise, as in the neighborhood of D, regions of bad crystal. The distance to which the bad crystal surrounding a dislocation extends is determined by the strength of the interatomic forces working to maintain the pattern of a perfect crystal. Hence, dislocations in a hard material are highly localized, while in softer materials, the region of bad crystal may extend for tens of interatomic distances from the dislocation center.

In a three-dimensional crystal, dislocations are linear defects. This will become evident when a second atomic plane is added to that
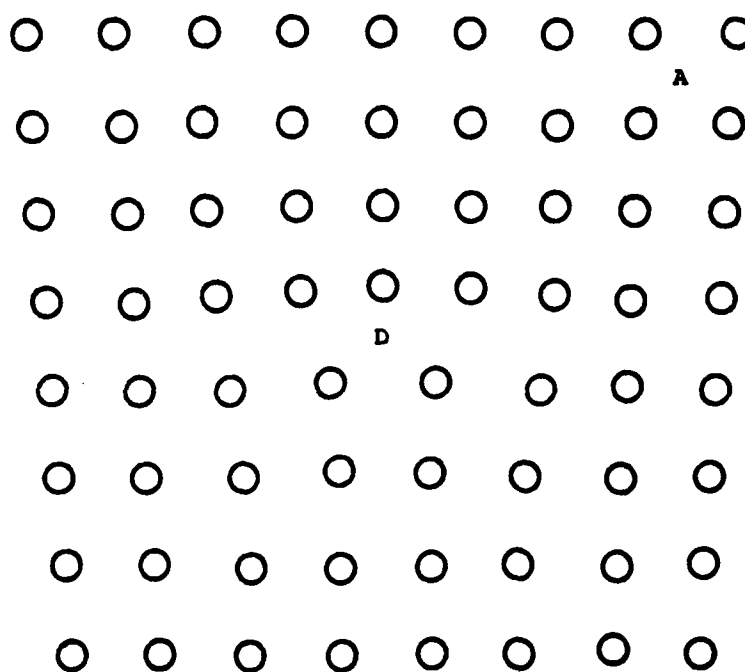
Figure 3. Atomic arrangement for an edge dislocation. D and A indicate regions of bad and good crystal, respectively.

in Figure 3. If atoms in this plane are arranged so as to maintain
the crystal pattern near the perimeter of the illustration, then a
misalignment of the atoms in the area above D is unavoidable. The
same holds for a third atomic plane, and so on. The dislocation must
therefore extend through the crystal along a line, though not neces-
sarily a straight one. A dislocation may terminate either at the
crystal surface, or within the crystal at a junction of dislocations.
The dislocation shown in Figure 3 is referred to as an edge disloca-
tion, since it can be viewed as occurring at the edge of a half-plane
of atoms which was inserted into a formerly perfect crystal. This is
shown more clearly in Figure 4c.

In Figure 4, a perfect crystal is compared to one containing an
edge dislocation. The closed circuit ABCDA in Figure 4a (referred
to as a Burgers Circuit) is made up of atom-to-atom steps along lat-
tice vectors. In Figure 4b, the same sequence of atom-to-atom steps
forms the circuit $A'B'C'D'E'$ which, as a consequence of the disloca-
tion it encircles, is not closed. That vector which must be added
to the real crystal Burgers circuit in order to close it, i.e., the
vector $\vec{E'A'}$ is called the Burgers vector $(\vec{b})$ of the dislocation. To
be included in the definition of the Burgers circuit is the require-
ment that it pass only through regions of good crystal. This being
the case, it is obvious that the Burgers vector must be a crystal
lattice vector (it is generally equal to one of the basis vectors of
the crystal lattice), and that the Burgers vector is independent of
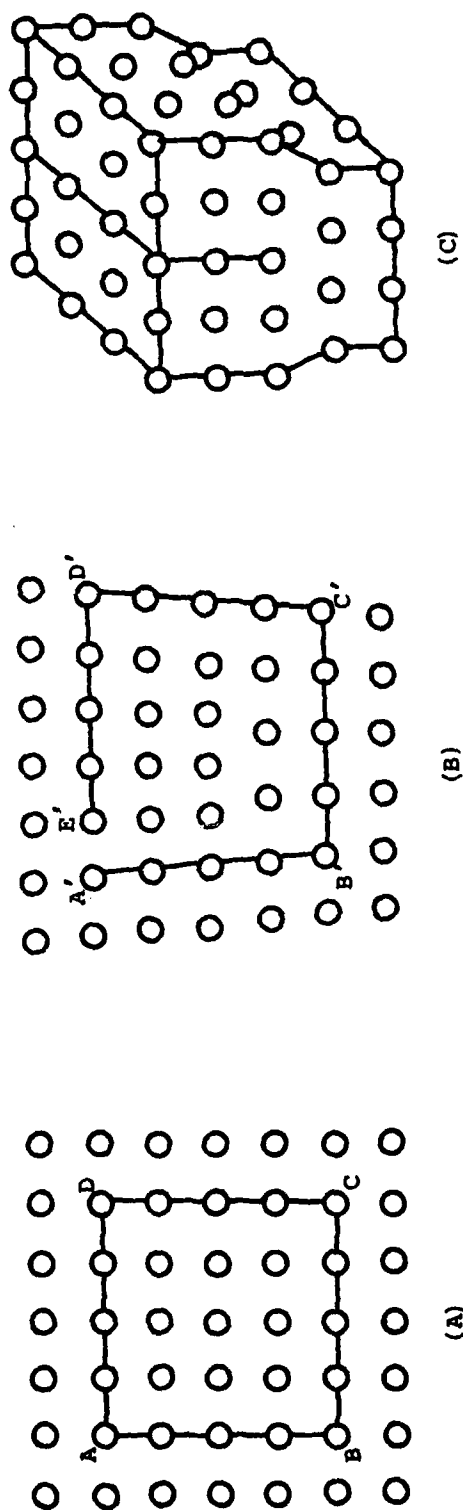
Figure 4. Atomic arrangement for an edge dislocation compared to that of a perfect crystal.

the particular circuit chosen, being solely determined by the encircled dislocation. Burgers (1939) has shown that a dislocation is uniquely characterized by its Burgers vector.

In Figure 4b, the Burgers vector is perpendicular to the dislocation line ($\vec{\ell}$) which extends normal to the surface of the figure. This is characteristic of edge dislocations. There can also be a situation, shown in Figure 5, in which the Burgers vector is parallel to the dislocation line. In this case, completion of the burgers circuit ABCDE which would be closed in a perfect crystal, requires a displacement along the direction of the dislocation line. Because of the screw-like nature of this circuit, defects of this type are known as screw dislocations. In general, the line of a dislocation may make any angle with the dislocation's Burgers vector. An arbitrary dislocation can always be considered as the sum of a pure screw ($\vec{\ell}\|\vec{b}$) and a pure edge ($\vec{\ell}\perp\vec{b}$) dislocation. The curved dislocation in Figure 6 serves to illustrate this. At A, the dislocation is screw-like. At B, however, it is an edge dislocation. Note that it is the direction of the dislocation line which changes; the Burgers vector is constant along the entire length of the dislocation.

Dislocations are mobile defects, travelling through the volume of a crystal by means of atomic rearrangements within the region of bad crystal. It is possible to distinguish two types of motion. The more difficult, climb, is illustrated in Figure 7. Here, the dislocation has moved from point D to D' by the small displacements of
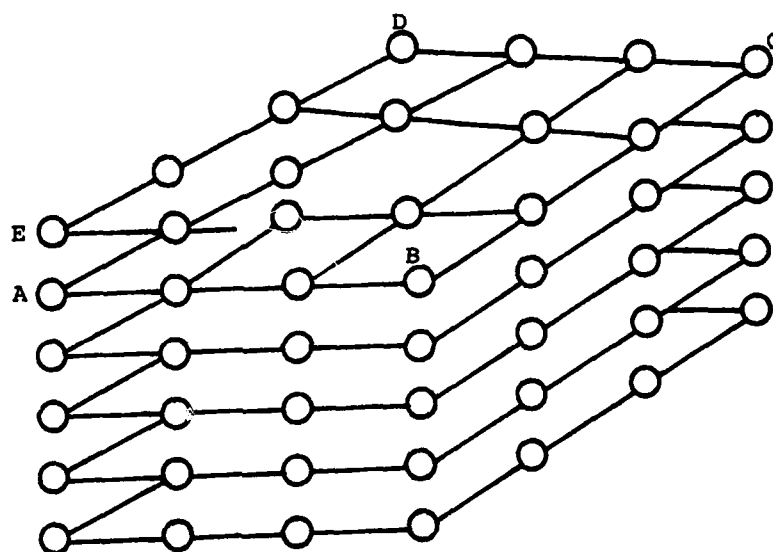
Figure 5.   Atomic arrangement for a screw dislocation.
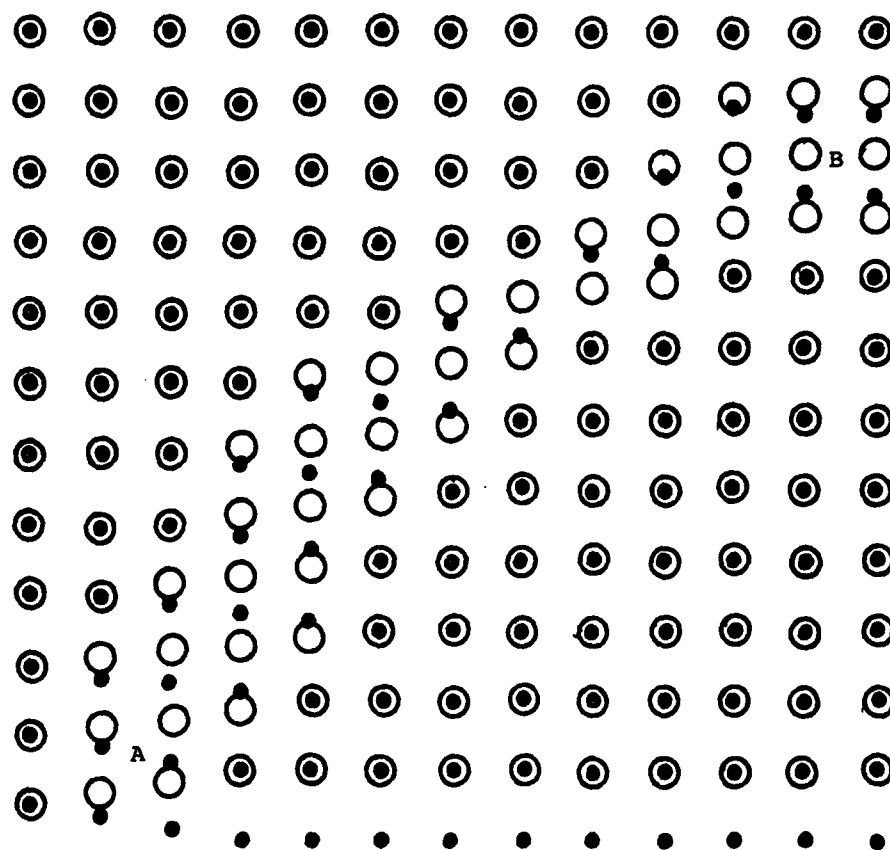
Figure 6. Atomic arrangement for a curved dislocation. Closed circles represent atoms below the slip plane and open circles those above it. The dislocation is screw-like at point A and edge-like at point B.
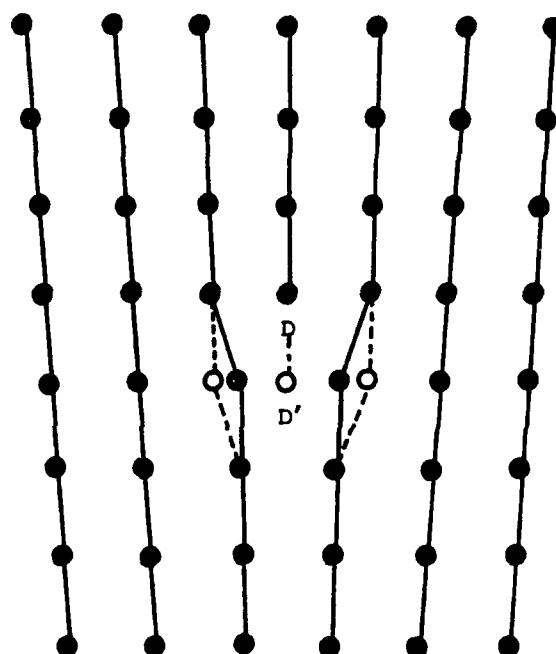
Figure 7. Atomic displacements corresponding to dislocation
climb.   Open circles represent atom positions
after the motion from D to D'.

a few atoms and, most significantly, by the addition of an atom to the crystal lattice. The extra atom essential to this process must be obtained either from interstitial atoms already present within the crystal, or by the creation of an atomic vacancy elsewhere in the crystal. The diffusion of atoms or vacancies through a crystal is such a slow process that the requirement of mass transport severely limits this type of motion.

The other manner in which a dislocation moves, glide, is shown in Figure 8. This process, which involves only the small displacement of a few atoms without the necessity of mass transport, is preferred to that of climb. The ease with which a dislocation glides is primarily determined by the width of the dislocation. By dislocation width is meant that length in the direction of glide over which the atoms are out of register by some prescribed amount. Figure 9 compares the motion of a wide and a narrow edge dislocation undergoing equal translations. In the case of the wider dislocation, more atoms are involved in the process. Consequently, the displacement required of each atom, and thus the resistance to glide, is less than for a narrow dislocation. Nabarrow (1947) has shown that the dislocation mobility increases by several orders of magnitude and the width of the dislocation is doubled. A dislocation's width is determined by the strength of the atomic bonds acting between those planes of atoms along which the dislocation glides. The stronger these bonds act to maintain the regular crystal pattern, the more narrow will be the dislocation. Since the forces binding the closely
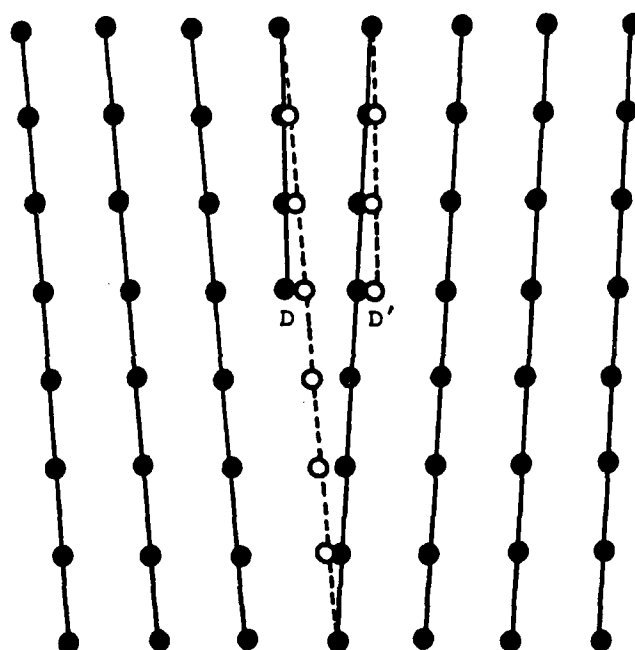
Figure 8.   Atomic displacements corresponding to dislocation
glide.   Open circles represent atom positions after
the motion from D to D′.
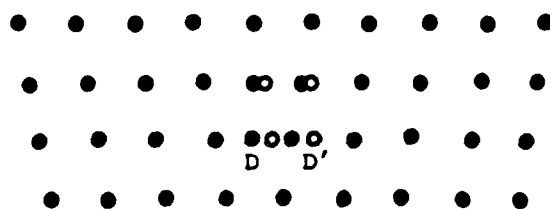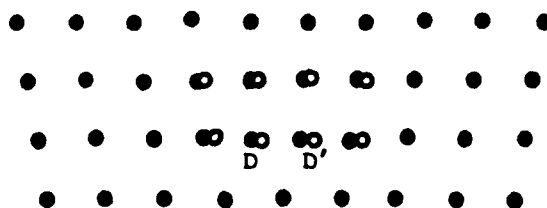
Figure 9. Comparison of atomic displacements corresponding to the glide of a narrow (A) and a wide (B) dislocation. Open circles represent atom positions after the motion from D to D'.

packed planes of a crystal are significantly less than those between other crystal planes, a dislocation gliding along these planes will be wider and hence more mobile than other dislocations in the crystal.

As Figures 7 and 8 illustrate, an edge dislocation climbs in a direction parallel to the additional half-plane of atoms, and glides in a direction perpendicular to this plane. The motion of an edge dislocation in some arbitrary direction may be viewed as the sum of a climbing and a gliding motion. Screw dislocations, by virtue of their axial symmetry, do not climb, but move in any direction by glide alone. As was the case with edges, a screw dislocation will be widest, and thus most mobile, along the closely packed planes of the crystal. So dominant is the motion in these planes that both climb and glide along other planes can be disregarded. Those planes along which this predominant glide takes place are referred to as the glide planes of the crystal.

Dislocations will move when an external stress is applied to the crystal. Figure 10 illustrates the manner in which a gliding disloca- tion allows the crystal to yield to an applied stress(σ). As the dis- location moves through the body, the material above the glide plane is displaced with respect to that below by an amount equal to the Burgers vector ($\vec{b}$). Consider, as in Figure 11, a sheared crystal in which a length (ℓ) of dislocation moves a small distance (x). That part of the crystal which is displaced during this process has a surface area ℓx on which the shearing force is $\sigma \ell x$. The work done on
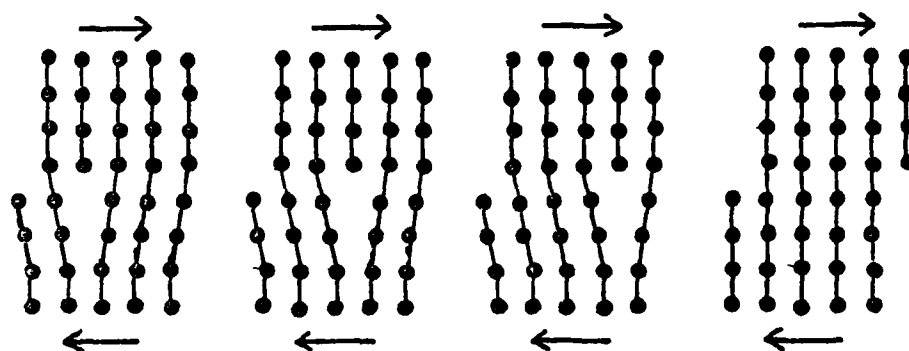
Figure 10. Crystal yield by means of dislocation displacement.

this surface during its displacement (which is also the work done on the crystal itself) is equal to $\sigma \ell x b$. This dependence of the work on the dislocations position indicates that there is a force on the dislocation equal to σb per unit length. In general, the force on a dislocation with Burgers vector $\vec{b}$ is given by:

$$\vec{F} = \vec{\nu} \times (\vec{b} \cdot \vec{\sigma}) \tag{2.1}$$

(Peach and Koehler, 1950),where $\vec{\nu}$ is a unit vector tangent to the dislocation,and $\vec{\sigma}$ (a tensor) is the stress applied to the crystal. This force,$\vec{F}$ above, is to be viewed as acting upon the dislocation line itself, considered as a distinct physical entity. The response of the dislocation to this force is determined by the inertia of the surrounding atoms whose actual displacements constitute the dislocation motion. It is reasonable,then, to attribute to the dislocation itself an inertia of approximately the same magnitude as that of a row of atoms, i.e., ρa^2 per unit length, where ρ is the mass density of the crystal,and a is the interatomic distance. Various authors derive slightly different expressions for the effective mass of a dislocation (see, for example, Brailsford, 1966). For the purpose of this work, the effective mass per unit length is taken to be that used by Granato and Lücke (1956) which is $\pi \rho b^2$.

It is convenient, at this point, to indicate the crystal strain that results from the motion of a dislocation. Consider the situation of Figure 11. As the dislocation moves, sweeping out an area A in the glide plane, an equivalent area on the crystal's surface undergoes a displacement b. The average displacement of the crystal's
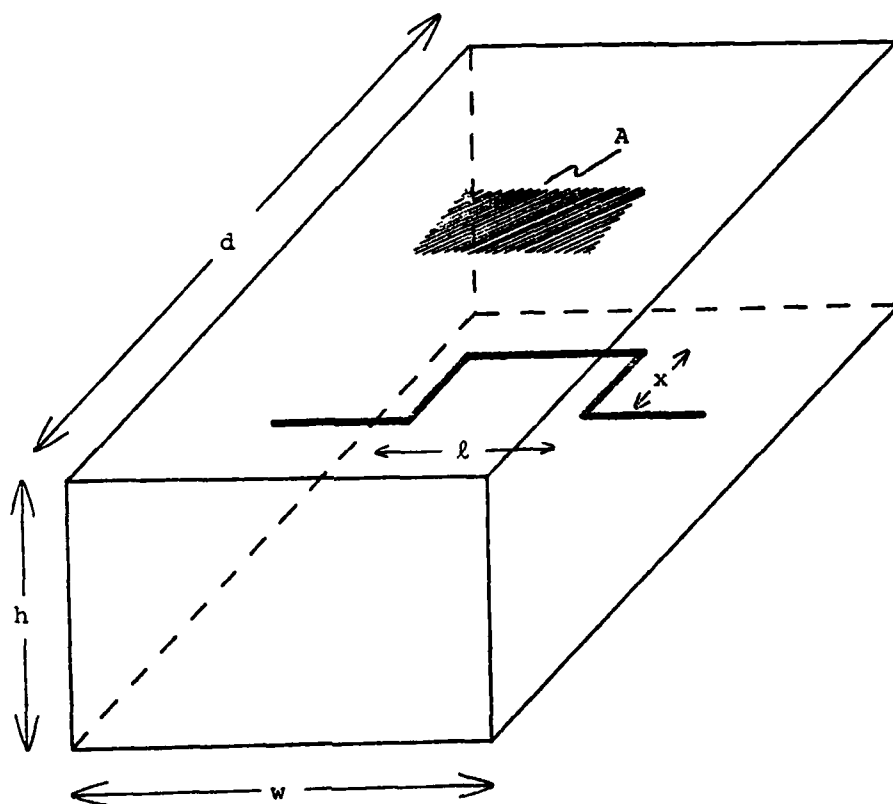
Figure 11.   Dislocation displacement within a crystal.

surface is then bA/wd. The crystal strain, which is pure shear, is given by bA/wdh, equal to bA/V, where V is the crystal volume. This result will be of use later in the chapter.

The internal energy of a crystal which contains either a dislocation or an impurity atom is greater than that of an equivalent perfect crystal. The difference in energies, equal to the work that must be done to distort a perfect crystal's regular atomic scheme into the configuration of a real, defect bearing crystal, is termed the misfit energy. The crystal system, acting in such a way as to minimize this misfit energy, endows the dislocation with properties relevant to this study. The first is the propensity of a dislocation to maintain a straight-line configuration. By minimizing the dislocation length, the volume of bad crystal, and hence, the misfit energy, is minimized. It is thus both convenient and valid to view the dislocation as having a line tension which, when the dislocation is curved, produces a side-wise restoring force. Several authors (see Read and Brailsford, 1974) have calculated this line tension and find that it is approximately $\frac{1}{2}$ Gb^2, where G is the shear modulus of the crystal. Secondly, dislocations will be pinned at the sites of impurity atoms (Cottrell, 1948). For a crystal which contains both an impurity atom and a dislocation, the misfit energy is reduced if the two defects are made to coincide. Since work must be done on the impurity-dislocation defect to separate the two, there is a force which binds them together. If any external force is applied to the dislocation, it is possible for the dislocation to move while dragging the impurity

atom with it. However, this is a slow process and does not need to be considered in this study. An external force which is larger than the pinning force will cause the dislocation to break away from the impurity atom. This situation can be avoided experimentally by limiting the magnitude of the stress applied to the crystal.

There remains to be considered one other force which acts upon a dislocation. This is a drag resulting either from the interaction of a moving dislocation with electrons and phonons, or from the radiation of energy by an accelerating dislocation. Electrons or phonons which impinge on a dislocation are scattered by the inhomogeneous strain field and density near the dislocation center, thereby exerting a force on the dislocation. If the distribution of particle velocities is isotropic, then the net force on a stationary dislocation will be zero. When the dislocation is moving, however, more particles are encountered on its leading side than on the trailing side, and so it experiences a net force opposing the motion. In addition to this, if the dislocation is undergoing an acceleration, it will radiate energy in the form of elastic waves. For the dislocation to lose energy in this manner is equivalent to its working against an additional damping force. In each of these cases, the drag force is found to depend linearly on the velocity of the dislocation. The damping force on an oscillating dislocation may therefore be expressed as:

$$\vec{F} = -(B_p + B_e + B_r)\vec{v} \quad , \tag{2.2}$$

where B_p, B_e, and B_r are, respectively, the phonon, electron, and radiation drag coefficients, and $\vec{v}$ is the velocity of the dislocation. Various expressions for the drag coefficients are derived in the literature. Leibfried (1950) has calculated the phonon contribution and finds that the drag coefficient varies as T^5 below the Debye temperature. By all accounts, at liquid helium temperatures, the phonon drag is negligible. Brailsford (1969) has determined that the electronic drag coefficient is temperature independent, but is proportional to the free electron density in the crystal. Specifically, B_e varies as the number of conduction electrons which are not bound in Cooper-pairs. In the non-superconducting state, B_e is constant. For a metal which is in the superconducting state, however, B_e will vary with temperature as does the density of quasiparticles according to an expression derived in the BCS theory of superconductivity. The final drag term, that due to radiation losses, has been studied by Garber and Granato (1970) for the case of an oscillating dislocation. They find that the radiation drag coefficient is simply given by $A\omega/8$, where ω is the angular frequency of the oscillation, and A is the effective mass per unit length of dislocation. The damping force on a dislocation may therefore be expressed as:

$$\vec{F} = -B(\omega,T)\vec{v} \qquad (2.3)$$

and

$$B(\omega,T) = B_0 \, \beta(T) + A\omega/8 \quad , \qquad (2.4)$$

where B_0 is a constant, and $\beta(T)$ is the temperature dependent BCS quasiparticle density.

The justification for the Koehler model is now evident. Dislocations exhibit properties of mass, tension, viscous drag, and endpoint pinning that are identical to those of a taut string. A study of the dynamics of an oscillating dislocation may therefore follow the example set by classical studies of an oscillating string.

B. Dislocation Damping Theory of Granato and Lücke

Granato and Lücke's (1956) calculation of the ultrasonic attenuation caused by crystal dislocations is based on Koehler's (1952) suggestion that the motion of a segment of dislocation is equivalent to that of a taut string. Since these two systems exhibit identical properties of mass, tension, viscous drag, and endpoint pinning, it is expected that a dislocation will obey the equation of motion for a string given by Rayleigh (1894). For an element of unit length, this equation is:

$$A \frac{\partial^2}{\partial t^2} \xi + B \frac{\partial}{\partial t} \xi - C \frac{\partial^2}{\partial y^2} \xi = F \quad . \tag{2.5}$$

In this expression, A is the effective mass, B is the damping coefficient, and C is the effective line tension. F is the driving force on the dislocation. ξ is the displacement of the dislocation from its equilibrium position. The coordinate system is chosen such that the undisplaced dislocation lies parallel to the y-axis and the dislocation glide is in the x-y plane (see Figure 12). The force which drives the dislocation is determined from the stress being applied to the crystal using Equation (2.1). The only component
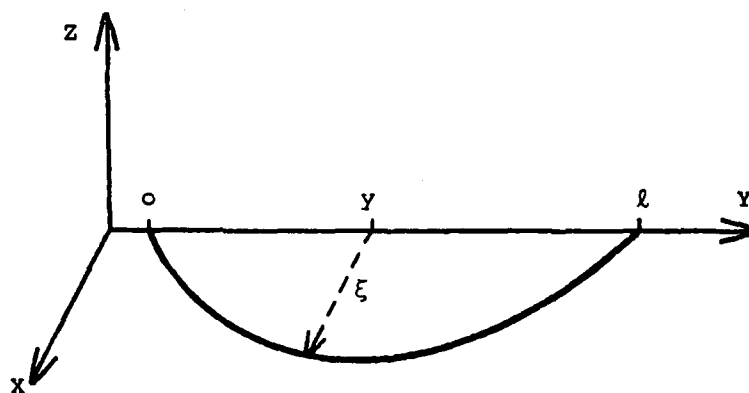
Figure 12.   Displacement of a bowed dislocation.

of the applied stress which will be effective in causing dislocation motion is a shear normal to the dislocation and in the glide plane of the crystal, i.e., along the x-axis in Figure 12. Other stress components have negligible effect on the dislocation and need not be considered. Of all the possible stresses which may be used, the one of interest corresponds to a longitudinal sound wave. In this case,

$$\sigma = \sigma_0 \, e^{-\alpha x} \, e^{i(\omega t - 2\pi x/\lambda)} \quad . \tag{2.6}$$

Here, σ_0 is the effective stress amplitude. ω and λ are, respectively, the sound wave frequency and wavelength. α, the attenuation coefficient, describes the rate at which the stress is diminished as it passes through the dislocation bearing crystal. The driving force on the dislocation is given by:

$$F = b\sigma \quad . \tag{2.7}$$

In general, the dislocation displacement will be a function of three space coordinates and time. In the problem just described, however, there is no z-coordinate dependence and we write $\xi = \xi(x,y,t)$. Combining Equations (2.5), (2.6), and (2.7) gives the dislocation equation of motion as:

$$A \frac{\partial^2}{\partial t^2} \xi(x,y,t) + B \frac{\partial}{\partial t} \xi(x,y,t) - C \frac{\partial^2}{\partial y^2} \xi(x,y,t) = b\sigma_0 e^{-\alpha x} \, e^{i(\omega t - 2\pi x/\lambda)} \quad .$$

$$\tag{2.8}$$

The displacement is subject to the boundary conditions

$$\xi(x,o,t) = \xi(x,\ell,t) = 0 \qquad (2.9)$$

imposed by the endpoint pinning. In Appendix A, it is shown that a solution to this equation is:

$$\xi(x,y,t) = \frac{4b\sigma_0}{A\pi} e^{-\alpha x} \sum_{n=0}^{\infty} \frac{1}{(2n+1)} \sin\frac{(2n+1)\pi y}{\ell} \frac{e^{i(\omega t - 2\pi x/\lambda - \delta_n)}}{\left[\left((2n+1)^2\omega_0^2 - \omega^2\right)^2 + \left[\frac{B}{A}\omega\right]^2\right]^{1/2}} ,$$

$$(2.10)$$

where

$$\delta_n = \arctan\left(\frac{\frac{B}{A}\omega}{(2n+1)^2\omega_0^2 - \omega^2}\right)$$

and

$$\omega_0 = \frac{\pi}{\ell}\left(\frac{C}{A}\right)^{1/2}$$

is the resonant frequency of the dislocation loop.

The contribution of dislocations to the ultrasonic attenuation is determined in the following manner. Consider an element of crystal which contains a dislocation and is subjected to an external stress. The equation of motion for this system is:

$$\nabla^2\sigma - \rho\frac{\partial^2}{\partial t^2}\varepsilon = 0 \qquad , \qquad (2.11)$$

where ε is the crystal strain. This strain is made up of two kinds, the elastic strain and an additional strain due to the motion of dislocations, i.e.,

$$\varepsilon = \varepsilon_{el} + \varepsilon_{dis} \quad . \tag{2.12}$$

The elastic strain is:

$$\varepsilon_{el} = \sigma/G \quad , \tag{2.13}$$

where G is the shear modulus of the crystal. In a unit volume of crystal, the dislocation strain is given by:

$$\varepsilon_{dis} = b \int_{0}^{\ell} \xi(x,y,t) \; dy \; , \tag{2.14}$$

where, using the notation of Figure 12, this integral is the area swept out by the moving dislocation. Substitution of Equations (2.12), (2.13), and (2.14) into Equation (2.11) allows that equation of motion to be written as:

$$\nabla^2 \sigma - \frac{\rho}{G} \frac{\partial^2 \sigma}{\partial t^2} = \rho b \frac{\partial^2}{\partial t^2} \int_{0}^{\ell} \xi(x,y,t) \; dy \quad . \tag{2.15}$$

This equation is solved simultaneously with those for the applied stress [Equation (2.6)] and the dislocation displacement [Equation (2.10)] in order to obtain an expression for the attenuation coefficient, α. The result, derived in Appendix A, is:

$$\alpha = \frac{8\ell^3 \omega}{v\pi^4} \sum_{n=0}^{\infty} \frac{1}{(2n+1)^2} \frac{D\Omega}{\left[(2n+1)^2 - \Omega^2\right]^2 + D^2\Omega^2} \quad , \qquad (2.16)$$

where $\quad D = \dfrac{(B/A)}{\omega_0}$, $\quad \Omega = \dfrac{\omega}{\omega_0}$ and $\quad \omega_0 = \dfrac{\pi}{\ell} \left(\dfrac{C}{A}\right)^{1/2}$.

In the literature, it is customary to discuss the acoustic characteristics of dislocations in terms of decrement (Δ) rather than attenuation (α). The decrement is defined as the ratio of the energy lost per cycle to twice the total vibrational energy stored in the specimen. It is simply related to the attenuation by the equation

$$\Delta = \frac{2\pi v}{\omega} \alpha \quad ,$$

where α is measured in nepers per cm. Following this convention, Equation (2.16) is rewritten as:

$$\Delta_\ell = \frac{16 \, \ell^3}{\pi^3} \sum_{n=0}^{\infty} \frac{1}{(2n+1)^2} \frac{D\Omega}{\left[(2n+1)^2 - \Omega^2\right]^2 + D^2\Omega^2} \quad . \qquad (2.17)$$

Most authors have followed the example of Granato and Lücke, and assume that the first term in Equation (2.17) is an adequate approximation to the full series. The expression thus obtained is:

$$\Delta_{approx} = \frac{16 \, \ell^3}{\pi^3} \frac{D\Omega}{(1-\Omega^2)^2 + D^2\Omega^2} \quad . \qquad (2.18)$$

This approximation is justified by pointing out that if the ultrasonic frequency is on the order of the constant ω_0 or less, and the damping constant B is not too small, then higher order terms in the series go down as $(2n+1)^{-6}$. For frequencies higher than ω_0, however, the approximation may be a poor one, as a comparison of Figures 13 and 14 shows. Granato and Lücke further assume that the constant ω_0 will be of sufficient magnitude that $\Omega^2 \ll 1$ for all frequencies of interest. If this is the case, then Equation (2.18) reduces to

$$\Delta_{approx} = \frac{16\,\ell^3}{\pi^3} \frac{D\Omega}{1+D^2\Omega^2} \tag{2.19}$$

which, since it depends only on the product of D and Ω and not on their individual values, is a considerable simplification of the exact expression. Results similar to this have been obtained by other workers. Mason (1966), after presuming the bowed dislocation to have a parabolic shape and that $\Omega^2 \ll 1$, determines the dislocation decrement to be:

$$\Delta_{Mason} = \frac{\pi^3 \ell^3}{72} \frac{D\Omega}{1 + \frac{\pi^4}{144} D^2\Omega^2} \;. \tag{2.20}$$

Oen et al. (1960) consider the case of damping-limited dislocation motion (i.e., an inertia-free model) and obtain as an expression for the decrement

$$\Delta_{Oen} = \pi\ell^3 \frac{1}{\phi^3} \left[\phi - \frac{\sinh\phi + \sin\phi}{\cosh\phi + \cos\phi} \right] \;, \tag{2.21}$$
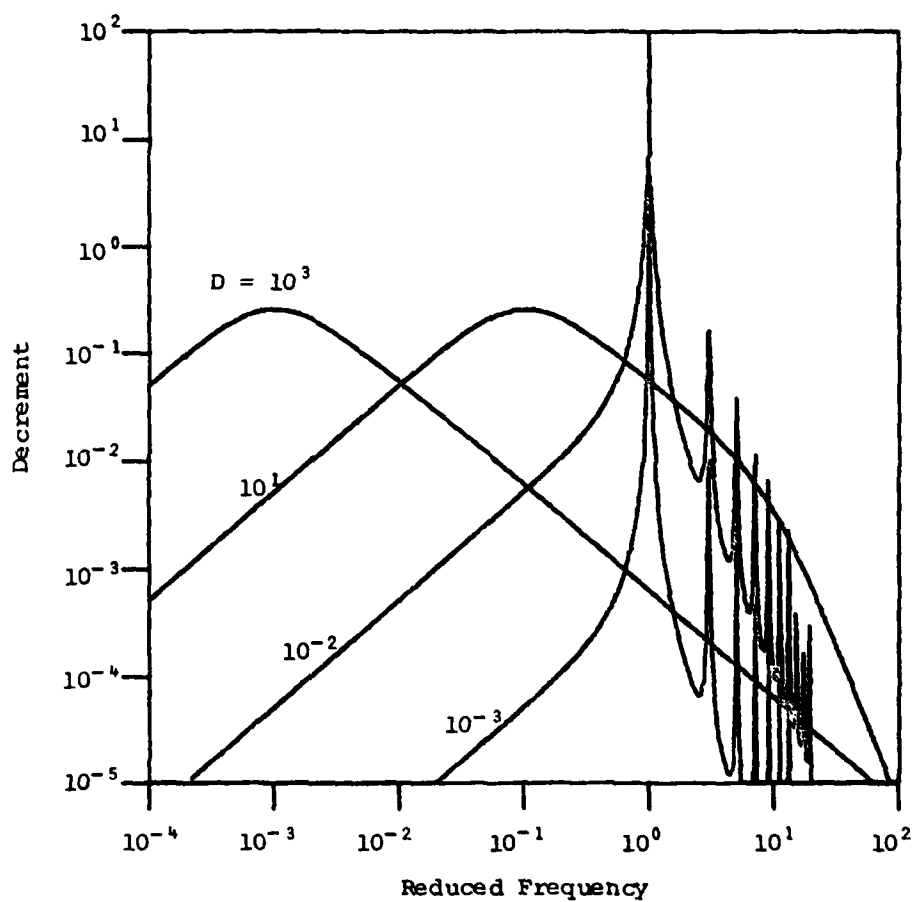
Figure 13. Complete series solution for the decrement by a single dislocation loop.
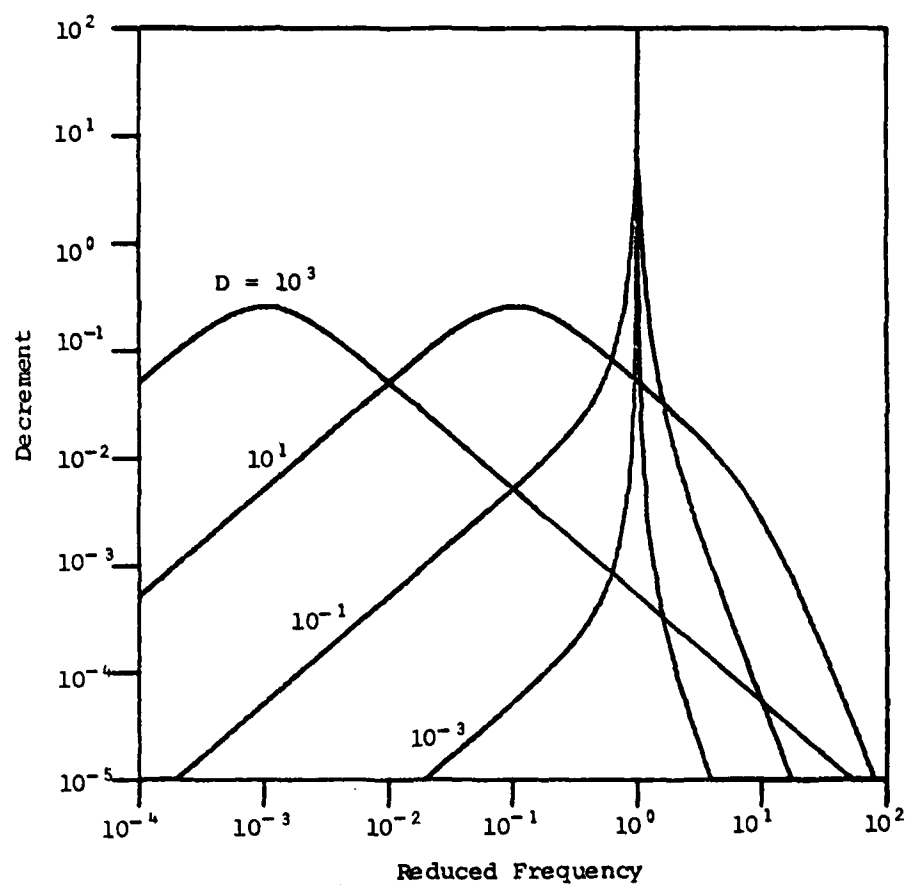
Figure 14. First term approximation to the solution for the decrement by a single dislocation loop.

where $\phi = \pi\left(\dfrac{D\Omega}{2}\right)^{1/2}$.

These three approximate solutions [Equations (2.19) through (2.21] do not differ significantly in their characters.

Since the validity of Granato and Lücke's approximations is not proven, the following calculations employ the exact expression (2.17) for the decrement. For the purpose of later discussions, however, the results obtained when the approximate expression (2.19) is used will also be presented.

Equation (2.17) gives the decrement for a single dislocation loop of length ℓ. Any real crystal will contain a large number of dis- locations having a wide variety of loop lengths. [A cubic centimeter of pure single crystal can be expected to contain on the order of 10^{12} dislocation loops whose average length is 10^{-4} cm (Mason, 1958).] The decrement that results from an assembly of dislocations is

$$\Delta = \int_0^\infty \Delta_\ell \ N(\ell) \ d\ell \ , \tag{2.22}$$

where $N(\ell) \cdot d\ell$ is the number of dislocations with lengths between ℓ and $\ell + d\ell$. The distribution of loop lengths is determined by the arrangement of pinning points (i.e., impurity atoms) along the dis- location line. It is generally expected that this pinning point arrange- ment will be a purely random one, in which case, the distribution

function for loop lengths will be given by (Koehler, 1952):

$$N(\ell) = \frac{\Lambda}{L^2} e^{-(\ell/L)} \quad , \tag{2.23}$$

where Λ is the total length of dislocation line per unit volume, and L is the average loop length. In Appendix B, it is shown that the net decrement that results from this distribution of loop lengths is given by either

$$\Delta = \Delta_0 \int_0^\infty \frac{x^5 \, D\Omega \, dx}{\sinh(x)\,[(1-\Omega^2 x^2)^2 + D^2\Omega^2 x^4]} \tag{2.24}$$

or by

$$\Delta = 2\Delta_0 \int_0^\infty \frac{x^5 \, e^{-x} \, D\Omega \, dx}{1 + D^2\Omega^2 x^4} \quad , \tag{2.25}$$

where

$$D = \frac{(B/A)}{\omega_0} \quad , \qquad \Omega = \frac{\omega}{\omega_0} \quad , \tag{2.26}$$

$$\omega_0 = \frac{\pi}{L}\left(\frac{C}{A}\right)^{1/2} \quad \text{and} \quad \Delta_0 = \frac{8\Lambda L^2}{\pi^3}$$

depending on whether the exact or the approximated expression [i.e., Equation (2.17) or (2.19)] for the single loop decrement is used for Δ_ℓ. In the final expressions for the decrement, the variable parameters are Ω, which is proportional to the ultrasonic frequency, and D, which varies with both frequency and temperature through the drag coefficient B. It is convenient at this time to indicate specifically

the frequency and temperature dependence of the parameter D. If the expression for B [Equation (2.4)] is substituted into the definition of D [Equation (2.26)] then one obtains:

$$D = D_0 \ \beta(T) + \frac{1}{8} \ \Omega \quad , \tag{2.27}$$

where D_0 is a constant.

Equation (2.24) is the final expression of the KGL theory. It specifies the manner in which the decrement is expected to vary with changes in ultrasonic frequency and dislocation drag. The integral in this equation, as well as the one in Equation (2.25), must be solved numerically. When this is done, the curves shown in Figures 15 and 16 are obtained.
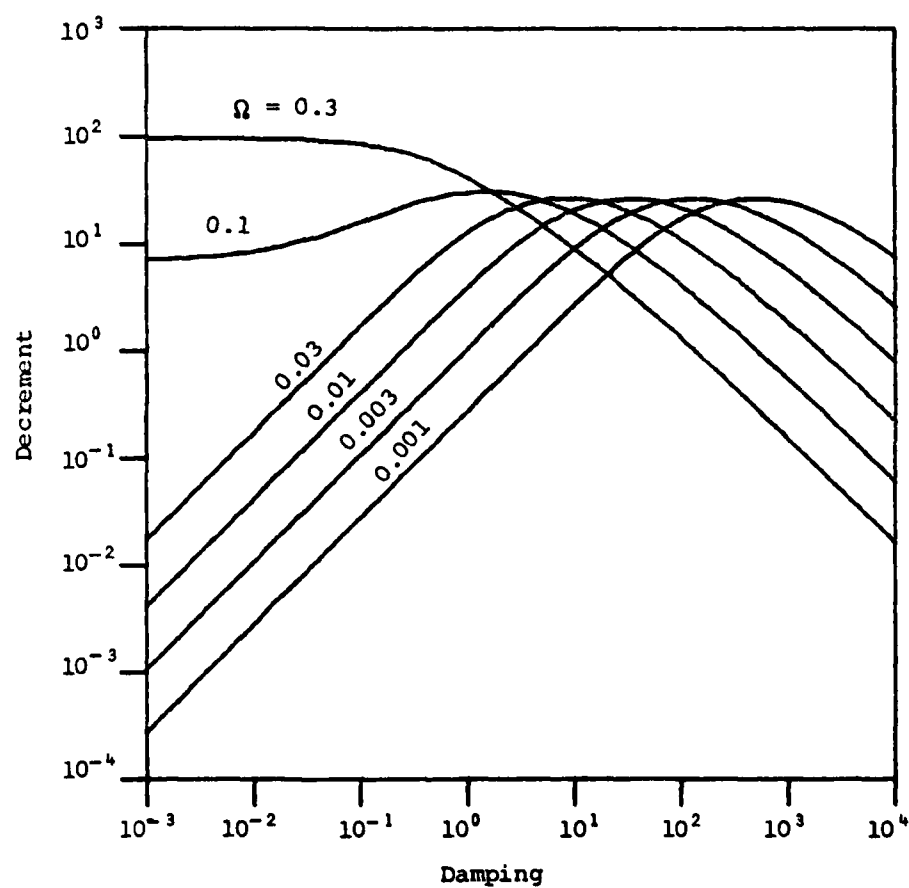
Figure 15.   Decrement for an assembly of dislocations at lower
frequencies.
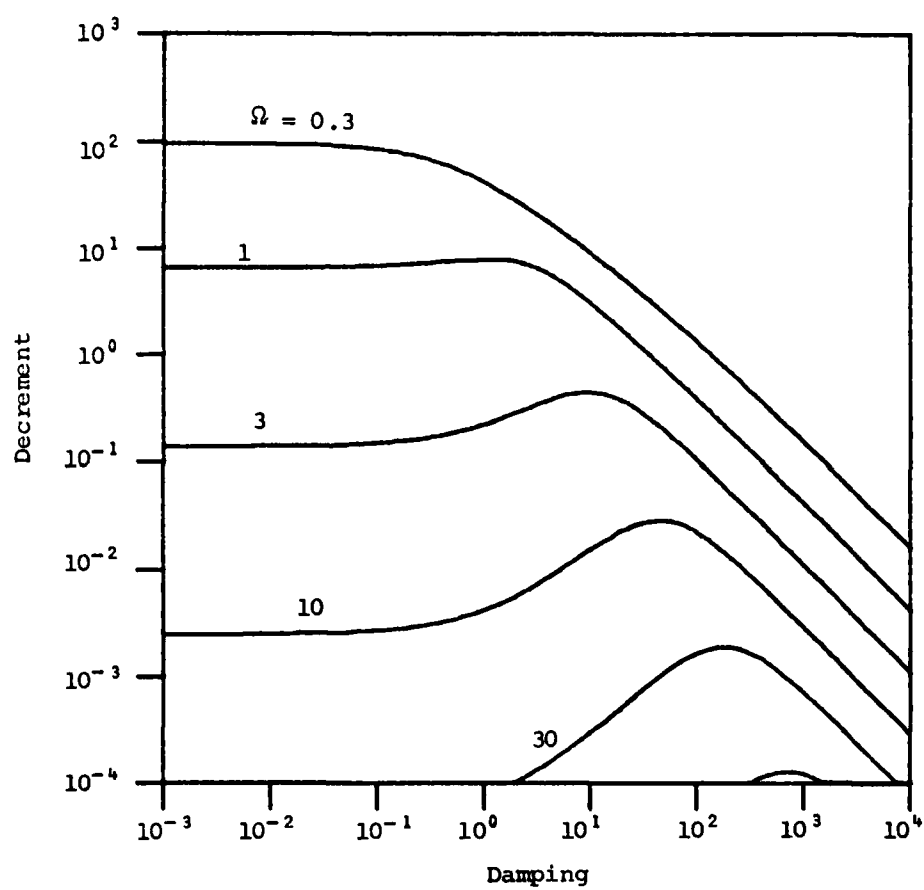
Figure 16. Decrement for an assembly of dislocations at higher frequencies.

III.   EXPERIMENTAL EQUIPMENT AND PROCEDURES

A.   Specimens

The specimens of indium employed in this study were taken from an ingot of MARZ grade indium (99.999% pure) purchased from the Materials Research Corporation. This ingot was approximately 1.3 cm in diameter, 10 cm in length, and was a single crystal of random orientation. The orientation of the crystal was determined by photographing x-ray diffraction patterns in the Laue-back-reflection method (Wood, 1963). The crystal was rotated on a two-circle goniometer until the photographed pattern was recognized to be that of a high symmetry crystal axis. The direction thus defined by the x-ray beam was identified as a particular crystal vector by comparison of the observed Laue pattern with those in the Laue Atlas (Preuss et al., John Wiley, 1974). By carefully symmetrizing the observed laue pattern through slight rotations of the crystal, the principle axes of the crystal were determined within one degree of arc. Two specimens were cut from this ingot, such that each specimen had flat, parallel surfaces perpendicular to a specific crystal vector. The two crystal vectors chosen for this study were along the [100] and [110] directions. These are the directions in the body-centered tetragonal (b.c.t.) system. A b.c.t. crystal may also be viewed as a face-centered tetragonal (f.c.t.) system (Cisney, 1959), in which case the direction indices are different.)

Indium is a very soft material, and great care must be taken to insure against damaging the crystal structure of a specimen during its preparation. The indium crystal was cut, and the specimen surfaces were planed on a Materials Research, Ltd., Servomet SMD, spark cutting machine. The details of this procedure are given by Binnie (1971). The Servomet SMD cuts and planes metal by means of an electric spark jumping between the work and a servo-controlled tool. During this operation, the work and tool are submerged in a kerosene bath which serves to cool the work and also provides a dielectric medium for the sparking. Surface damage to the specimen was minimized by using the lowest power spark available. Following the planing of the specimens, this surface damage, estimated to be 10 μm deep, was reduced by etching the specimens for 30 seconds in a 50% solution of nitric acid. The shape of the finished specimen was that of a 1.2 cm diameter cylinder with a length of approximately 1 cm. (The actual lengths of the specimens were 1.14 cm and 0.817 cm for the [100] and [110] crystals, respectively.) This length was used in order that the specimen exhibit a measurable net attenuation at the lowest ultrasonic frequency employed (2 MHz). Since the attenuation in a crystal varies as the frequency, there is an upper limit, dependent upon the specimens length, on the frequency of ultrasound that can be transmitted through a particular specimen. Had the experimental results warranted it, these specimens would have been shortened to allow the

collection of further data at frequencies higher than those eventually employed.

Two identical Valpey Fisher Corporation x-cut, 2 MHz, quartz transducers were bonded to the parallel surfaces of each specimen. These transducers produce purely longitudinal sound waves at the fundamental frequency and its odd harmonics. A small drop of Dow Corning 200 fluid, 600 stokes viscosity, was placed on the specimen surface. A transducer was then placed on top of this drop and gently pressed against the specimen to leave a thin, uniform film of fluid between the transducer and specimen surface. This pressure was maintained for several hours, and resulted in a very thin fluid film which, at room temperature, produced an "atmospheric pressure" bond that held the transducer in position during handling of the specimen. As the specimen was cooled to liquid nitrogen temperature, the fluid film solidified and the transducer was thus rigidly bonded to the specimen. Bonds made in this way could be cycled between liquid helium temperature and room temperature without deterioration.

B. Specimen Holder

The specimen holder illustrated in Figures 17 and 18 was used to suspend the specimen in a bath of liquid helium. The liquid helium cryostat was connected to a vacuum pumping system by which the temperature of the helium bath was lowered to approximately 1 Kelvin. The holder consists of a copper block which encloses
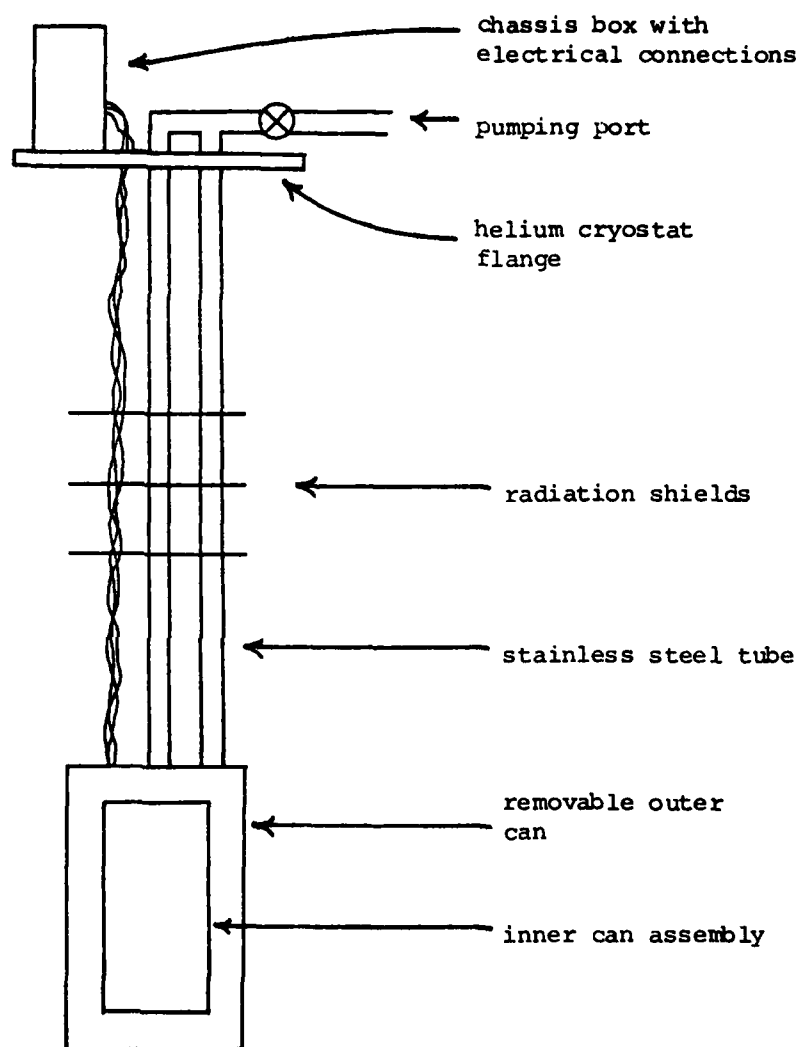
Figure 17. Schematic representation of the specimen holder.
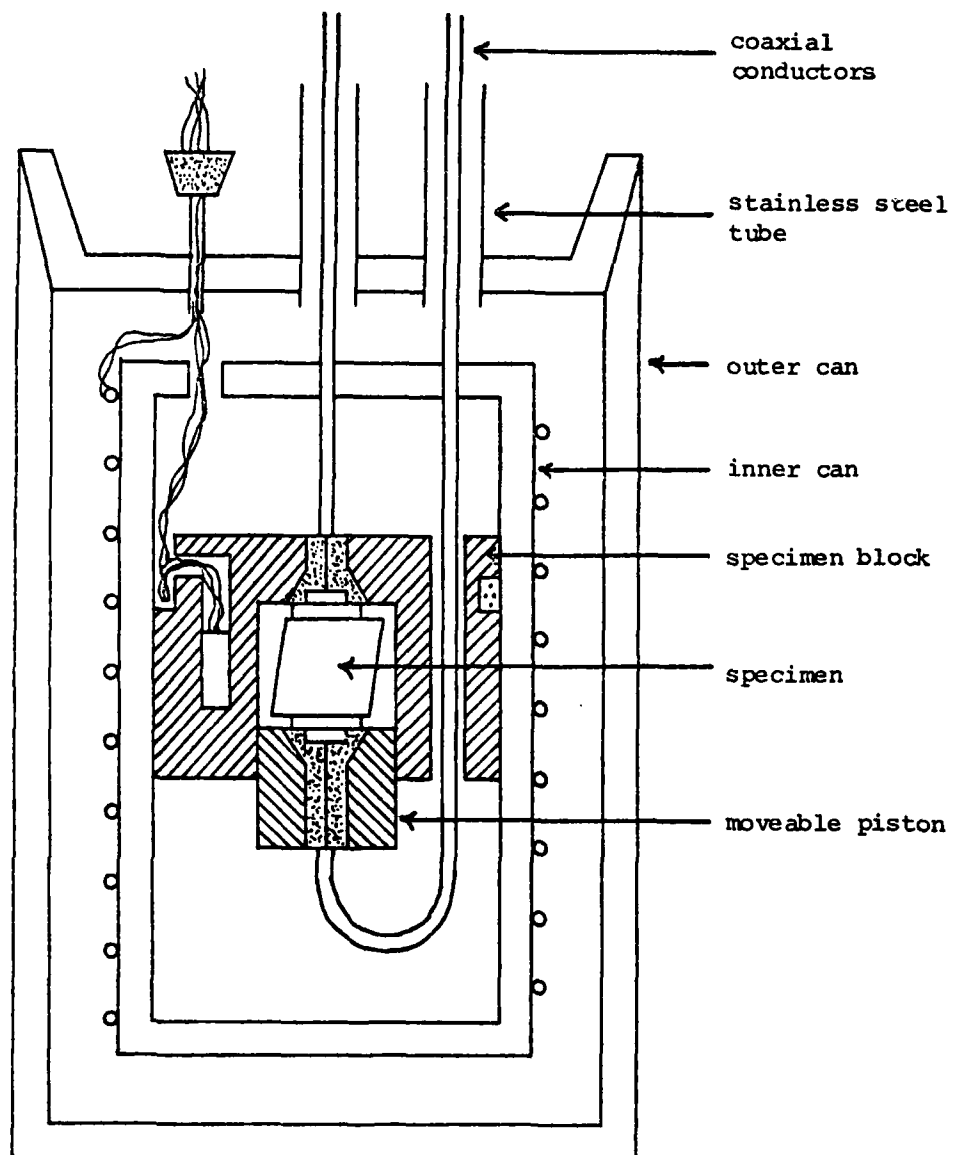
Figure 18. Details of the specimen holders lower assembly.

the specimen, and is itself enclosed by two coaxial cans. This assembly is hung by a pair of thin-wall stainless steel tubes from a flange which caps the helium cryostat. The two-can design allows a controlled variation of the specimen block temperature to any temperature above that of the helium bath. Elimination of the need to vary the bath temperature (through changes in the helium vapor pressure) in order to vary the specimen temperature has been a significant improvement to the procedure of this experiment. Copper radiation shields placed along the supporting tubes reduce the heat transfer to the helium bath. All electrical connections, with the exception of four rigid coaxial conductors to be described later, pass through the helium bath, thus eliminating heat transfer to the lower assembly. At the top flange, these wires exit the cryostat by an epoxy feed-through. The epoxy used was Stycast epoxy #2850 with #9 catalyst. An o-ring sealed fitting at the top flange provided access for a liquid helium transfer tube. Two carbon resistors (approximately 170 Ω at ambient temperature) placed along the supporting tubes act as liquid helium level indicators. An external electromagnet is used to generate a magnetic field at the specimen location when required. The lower assembly of the specimen holder is constructed entirely of non-magnetic materials in order to eliminate distortion in this field and to prevent any trapped flux from sustaining a non-zero residual field when the electromagnet is removed.

The outer can (made of brass) serves as a counter-dewar, thermally insulating the inner can and specimen block from the liquid helium

bath. This can and its conical plug have a precisely machined four degree taper joint which is sealed by an intersticial film of Dow Corning 200 Fluid, 600 stokes viscosity. The procedure for sealing the can is as follows. A thick layer of Dow Corning 200 Fluid is applied to both the tapered surfaces. The can is closed and then evacuated by means of the tubing which extends through the top flange to a vacuum pump connection. As the atmospheric pressure closes the joint, excess fluid is squeezed out and removed. The can is then cooled to liquid nitrogen temperature. At that point, the fluid has solidified to form an excellent vacuum seal. Electrical connections to the specimen block enter the outer can at a Stycast epoxy feed-through in the top of the can.

The inner can is designed to maintain a thermally homogeneous environment for the specimen block. This can is a copper tube with a syntane bottom and brass top. In order to minimize the mechanical (and hence, that part of the thermal) contact between the inner and outer cans, the direct contact has been limited to the electrical connections going to the specimen block. These include four rigid stainless steel coaxial conductors. The top of the inner can is supported by these four rigid conductors, and hangs approximately 1 cm below the top of the outer can. The inner can screws onto its top, thus allowing it to be removed whenever the specimen block must be handled. Other electrical connections to the specimen block pass through the top of the can at a small hole which also serves as a gas escape when the outer can is evacuated. The

thermal contact between the inner can and the specimen block is maximized by machining these pieces so that one fits quite tightly over the other. A coating of Dow Corning Silicone Grease between the contacting surfaces optimizes the thermal contact. A bifilar nichrome wire with 250 Ω net resistance was wound about the entire length of the inner can. This heating element was epoxied in place, and afterward the wall of the can was covered by several alternating layers of epoxy and paper tissue. In this way, the heater is made to have good thermal contact with the can, while the contact between the can and the gas surrounding it is reduced. The epoxy used was Hysol epoxy resin R9-2039 with H2-3561 hardener.

The temperature of the specimen block is determined by the balance of joule heating in the current carrying nichrome filament and of cooling by a partial pressure of helium exchange gas maintained in the outer can. The details of the temperature control will be given later.

The specimen block is a copper cylinder into which a cylindrical cavity has been machined. The specimen is confined in this cavity by a spring-loaded copper piston which has a diameter equal to that of the cavity. The dimensions of the cavity allow specimens up to 2 cm in length and 1.5 cm in diameter to be employed. Copper "buttons" in the parallel cavity and piston faces contact the transducers bonded to the specimen surfaces. The buttons are electrically insulated from the block by a layer of Stycast epoxy. Each button is connected to a pair of rigid, 3.2 mm diameter, 50 Ω impedance coaxial conductors

made of stainless steel and teflon. The cavity button is soldered directly to the rigid conductor while the piston is made moveable by an intervening connection of flexible copper coaxial conductor. Microcracks in the outer cylinder of the rigid conductors are pervious to superfluid helium which can also diffuse along the teflon insulation. In order to maintain a vacuum in the outer can at temperatures below the superfluid transition temperature, the rigid conductors pass through the vacuum lines connecting the outer can to the top flange, thus avoiding contact with the liquid helium bath. At the top flange, the rigid conductors exit the vacuum space through a flexible seal of General Electric Clear Silicone Auto Seal, and are attached directly to General Radio Type 874 coaxial connectors. During operation of the experiment, one of these is connected to a stub-tunner which allows impedance matching between the high impedance transducer and the 50 Ω coaxial cable.

A copper washer with outside diameter equal to that of the cavity and inside diameter greater than that of the transducer is attached to one surface of the specimen by a coat of silver conductive paint. This washer serves a four-fold purpose. It insures the placement of the transducers directly opposite the buttons, electrically grounds the specimen to the block, improves the thermal contact between specimen and block, and finally, acts to shield against the in-cavity radiation of radio-frequency signals from the input to the output buttons.

The temperature of the specimen was measured with a germanium resistance thermometer embedded in the specimen block. Since most of the heat transfer between the sensing element of the thermometer and the environment takes place through the thermometers electrical connections, the last 35 cm of these wires before the thermometer were either Stycast epoxied to the specimen block, or were contained within the block itself.

C. Temperature Measurement and Control

The germanium resistance thermometer (Cryocal, Inc., Model CR500, Serial No. 1150) used to measure the temperature of the specimen block has been calibrated by Binnie (1971) to within 0.01 Kelvin. This thermometer is a four-probe device in which the resistance of the sensing element (a germanium single crystal) varies from approximately 10 $K\Omega$ to 500Ω as its temperature changes from 1 K to 4.2 K. The temperature is determined by measuring the voltage drop associated with a constant current of 1.1908 μa through the element. This voltage is precisely amplified (10 x gain) by a Hewlett-Packard 740 B Differential Amplifier/Standard Voltmeter and is measured simultaneously on the x-axis of an x-y chart recorder and on a Kiethly 5-digit microvolt meter with digital output. The temperature corresponding to this voltage can be obtained by the interpolation of a temperature vs. voltage table calculated from the thermometer's temperature vs. resistance calibration for the case of a 1.1908 μa current through the element.

During operation of the experiment, the specimen block/inner can assembly is cooled by approximately 300 m Torr of exchange gas in the outer can. This is the gas pressure measured by a gauge at the pumping port above the top flange, when the helium bath temperature is approximately 1 K, and there is no current in the heater. It has been found that significantly less gas than this results in temperature instability, while more gas provides an excessive and wasteful transfer of heat to the helium bath. The specimen block is heated by a direct current of between 0 and 30 ma through the nichrome heater. This is sufficient to vary the temperature of the specimen from a low of approximately 1.2 K to above 3.4 K, the superconducting transition temperature of indium. A current ramp is used to increase (or decrease) the heater current at a prescribed rate. This rate, chosen to be slow enough that the data measuring systems are quasi-static and yet not so slow that inefficient use was made of the helium bath liquid, was such that approximately 20 minutes were required to sweep the temperature between 1.2 and 3.4 K.

D. Ultrasonic Apparatus

Of the two identical transducers bonded to the specimen, one is used to generate, and the other to detect, ultrasound. The apparatus used to generate, detect, and measure this ultrasound is diagrammed in Figure 19. A master timing circuit controls the operation of several components for which synchronization is necessary. The generating transducer is driven by a pulsed radio-frequency (rf) oscillator operating at an odd multiple of the transducer's natural frequency

Master Timer

r-f pulsed osc. → step atten. → prec. step atten.

r-f pulsed osc. → step atten. → specimen → junction

oscillo-scope ← video detector amp. ← wide-band amp. ← diode limiter

sample and hold

lock-in

x-y recorder

digital meter → punch control
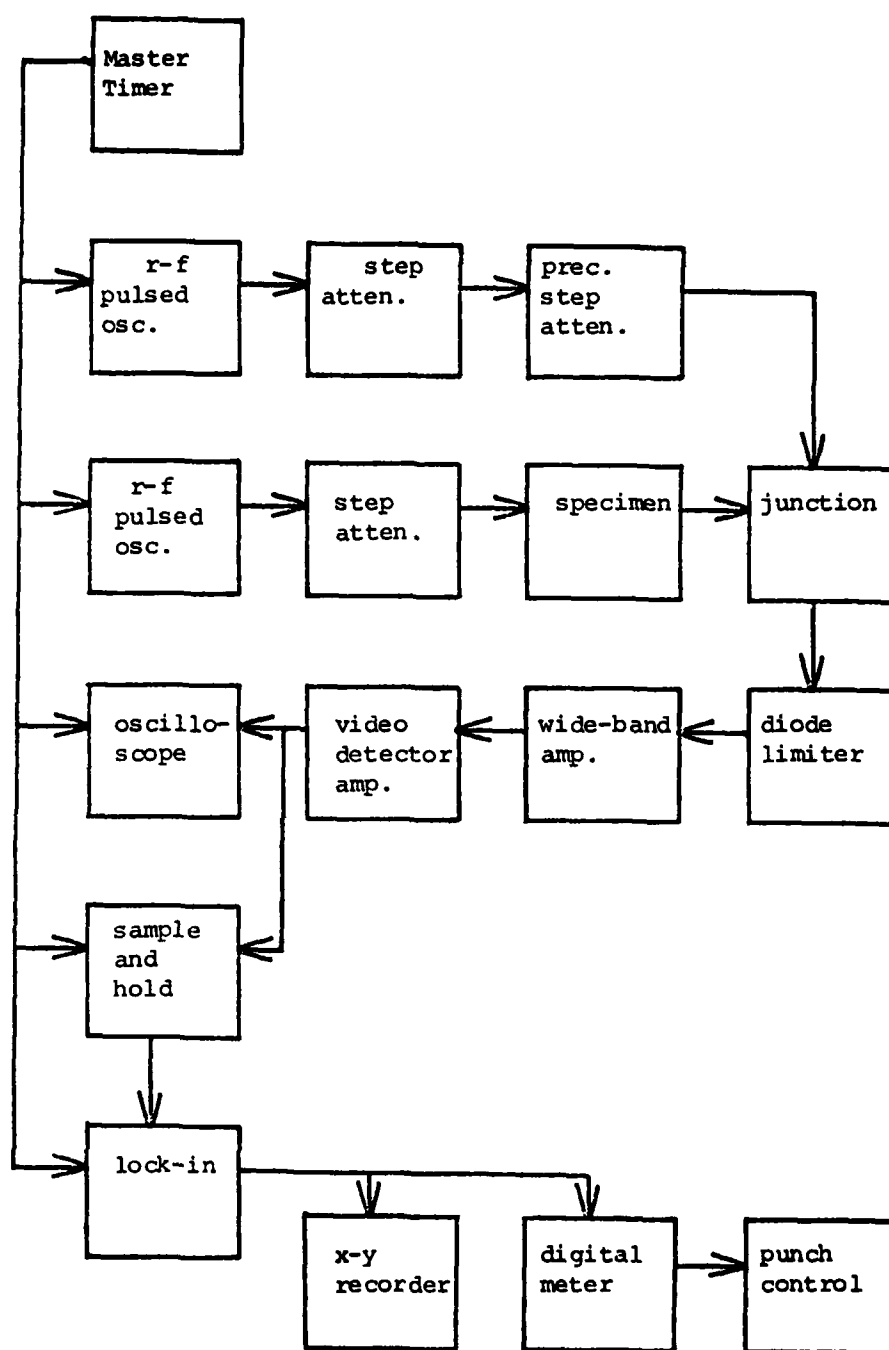
Figure 19. Block diagram of the equipment used to measure the relative ultrasonic attenuation.

(2 MHz). These rf pulses have a width of 1-2 μs and a 500 Hz repetition rate. Ultrasonic waves impinging on the detecting transducer produce small rf pulses which have amplitudes directly proportional to that of the ultrasound. These signals are processed by a wide-band rf amplifier followed by a video detector/amplifier. The rf amplifier is built of six cascaded Optimax Inc. modular amplifiers. These are three AH-401, followed by two AH-402, followed finally by a single AH-403. The input to this amplifier is protected from large signals (as might arise from leakage of the driving pulse) by a Micro-Dynamics MD-30L2 Coaxial Diode Limiter. The video detector/amplifier consists of a standard video detection circuit followed by a Burr-Brown 3554 wide-band operational amplifier. The rf transmission lines adjacent to the specimen holder include line-stretching segments that are tuned to optimize the signal reaching, or produced by, the transducers.

If the width of the driving pulse is less than twice the transit time for sound waves in the specimen, the detected sound waves will appear as exponentially decreasing "echos" of the initial pulse, which persists in the specimen through reflection at the specimens plane parallel surfaces. A typical video amplifier output for such a case is shown in Figure 20. The magnitude of the nth of these echo voltages indicates the sound wave amplitude after $2n-1$ transits through the specimen. The magnitude of a particular echo is measured by a sample-and-hold circuit (Computer Labs, THC-0300 Track and Hold).
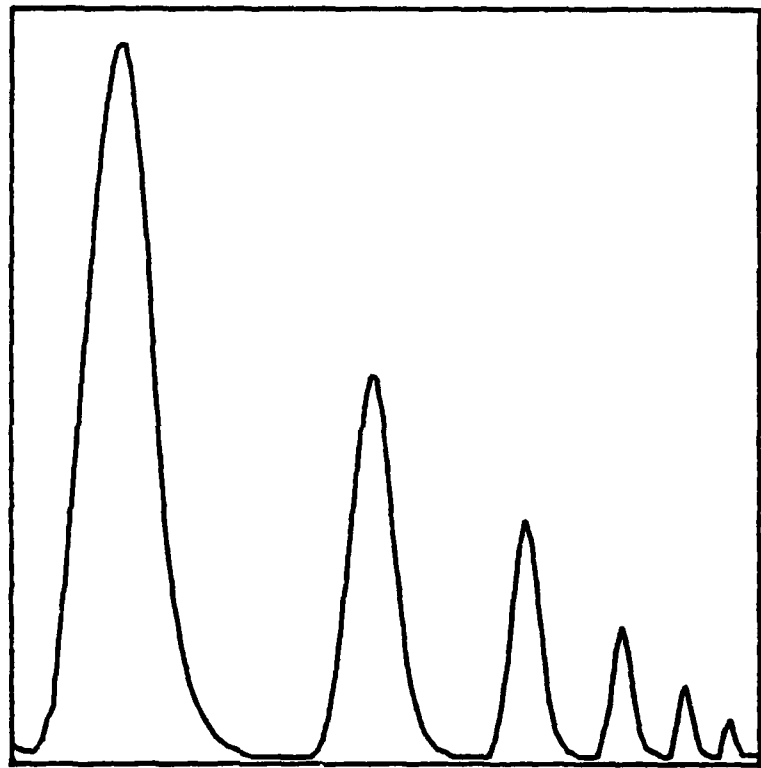
Figure 20. Ultrasonic pulse echo pattern.

This high speed circuit has a 100 ns wide gate which is set to coincide, in time, with the peak of the echo to be measured. The sampling rate, however, is twice the repetition rate of the pulsed oscillator so that the sample-and-hold circuit alternately measures the echo magnitude plus the video detected background noise and the level of the video detected background noise alone. The output of this circuit is therefore a square wave for which the peak-to-peak amplitude equals the magnitude of the echo peak voltage, and the frequency equals the repetition rate of the pulsed oscillator. This signal is input to a lock-in amplifier which measures the echo peak voltage, averaged over many cycles. (Typically, a 1.25-second time constant allows the averaging of 600 echo amplitudes). This averaged peak voltage, obtained from the lock-in output, is measured simultaneously on the y-axis of an x-y chart recorder and by a Digitec 4-digit millivoltmeter with digital output.

Changes in the ultrasonic attenuation of the specimen are observed as variations in the peak voltage of an echo. A correlation between the attenuation and the echo height is obtained by a pulse comparator calibration of the amplifier system. In this process, a pulsed signal from an auxiliary pulsed oscillator is substituted for the signal normally received from the detecting transducer. This substituted pulse is made equal to the original pulse in frequency, width and time delay, and is given an amplitude which is slightly greater than the maximum amplitude observed in the original pulse. The substituted pulse is then decreased in steps of known amount (approximately 1

decibel each) by a precision step attenuator (Weinschel Engineering, Model AD94-59-2, calibrated by the manufacturer to ± 0.05 dB) while corresponding values of the lock-in output are recorded. The substituted pulse is reduced until its amplitude is less than the minimum observed in the original pulse. A calibration of the relative attenuation vs. lock-in output is thus obtained. Absolute values of the attenuation, which cannot be measured in this way, are obtained by a process to be described later.

E. Recording of the Data

The principal data of this experiment, the ultrasonic attenuation as a function of temperature, is collected in the form of the ultrasonic echo peak voltage and the corresponding thermometer voltage. Two independent devices were used to record these data. The first is a punch system which simultaneously samples the digital outputs of the Digitec and Kiethly meters and records these values on a punched paper tape. In this form, the data are readily subjected to analysis by digital computer. The sampling rate was chosen to be approximately 20 per minute, as this was found to produce sufficient data points without overburdening the punch system. The data was also plotted on an x-y chart recorder. These charts serve as a permanent visual record of the collected data.

F. Procedure of the Experiment

During the entire experiment, the liquid helium bath is maintained at the lowest possible temperature, approximately 1 K. When collecting

a set of data, the initial situation has the specimen heated to a temperature of approximately 3.8 K (i.e., above the 3.4 K transition temperature of indium) and no applied magnetic field. The temperature is slowly decreased to approximately 1.2 K while the echo voltage and thermometer voltage are simultaneously recorded. The relative attenuation change is then calibrated by the pulse substitution method described earlier. After calibration, the original signal is reconnected and a magnetic field of approximately 400 Gauss is applied to the specimen causing it to be in the non-superconducting state, regardless of temperature. Data is collected again as the temperature is raised to 3.8 K. This complete temperature cycle and the associated measurements are referred to as a single data set, and approximately one hour is required for their collection. Each data set is duplicated one or more times, under identical conditions, as a test of the repeatability of the experiment.

Depending on the frequency and amplitude of the ultrasonic driving pulse, up to a dozen sonic echos may be seen in the normal state specimen. The attenuation data is recorded using one of the later echos available, thereby maximizing the total length of material through which the sound wave has passed. In this way, though the attenuation per unit length may have become small, the measured attenuation remains large. This serves to minimize the relative error in the attenuation calibration.

In order to avoid the possibility of amplitude-dependent effects influencing the data, measurements are made using as small a driving

pulse amplitude as practical. The absence of an amplitude dependence is guaranteed through the collection of equivalent data sets using various ultrasonic echos and (small) driving amplitudes, with the subsequent observation of no variation in the specimens attenuation per unit length.

During this experiment, secondary data were collected in order to determine the absolute attenuation at the lowest temperature obtained. In this case, the specimen is maintained at the minimum temperature while the sample-and-hold circuits gate delay is slowly increased from zero to some practical upper value. In this way, the gate sweeps through the "echo pattern" and the detection circuitry measures the signal shape as a function of time. The lock-in output is plotted on the y-axis of a time swept x-y recorder, producing a chart like the one shown in Figure 20. This data was not digitally recorded. After the pattern has been plotted, the system is again calibrated as described above. By thus measuring the ultrasonic attenuation after successive sound circuits through the specimen, an ..bsolute value for the attenuation is obtained. This value serves as a reference point by which the measured relative attenuations can be gauged. Unfortunately, this procedure is inherently less accurate than that used to collect the primary data, so that while relative attenuation measurements are quite reliable, absolute measurements are not. This will be discussed further.

IV. DATA ANALYSIS AND EXPERIMENTAL RESULTS

A. Data Reduction

A single set of the principle experimental data consists of two tables of ultrasonic echo peak voltage vs. thermometer voltage (one for the superconducting state and one for the normal state of the specimen) and a calibration table of relative attenuation vs. echo peak voltage. The echo and thermometer voltages were simultaneously measured at specimen temperatures which were arbitrarily distributed between 1.2 and 3.8 K. Analysis of this ta requires that it be in the form of pairs of attenuation values for normal and superconducting states of the specimen, corresponding to known values of temperature between 1.2 and 3.4 K. Reduction of the data to this form is accomplished by digital computer (IBM 370) using numerical inter-polation subroutine programs from the International Mathematical and Statistical Library of Subprograms, and employs a table of thermo-meter voltage vs. temperature obtained by numerical interpolation of the thermometer's resistance vs. temperature calibration. This table specifies the thermometer voltage corresponding to temperatures between 1.0 and 3.5 K in increments of 0.01 K.

The data reduction is a two-step process. First, the recorded tables of echo voltage vs. thermometer voltage are interpolated to obtain specifically the echo signals which would correspond to the specified thermometer voltages; i.e., to particular values of speci-men temperature. Then, the calibration table of relative attenua-tion vs. echo voltage is interpolated to obtain the attenuations

corresponding to these specific echo signals. When these attenuations are divided by the total distance transversed by the ultrasound [$(2n-1)\ell$, where n is the echo number, and ℓ is the specimen length], the result is a table of superconducting state and normal state attenuations per unit length vs. specimen temperature. Considering the precision of the IMSL interpolation subprograms and the great care given to accurate measurements of the echo and thermometer voltages, the principle source of error in the final values of attenuation and temperature is seen to be the calibrations of the precision step attenuator and the germanium resistance thermometer. The uncertainties which are thus associated with the reduced data are ±0.01 K and ±0.05 dB for temperature and net attenuation, respectively.

An experimental value of interest, the difference of attenuations in the normal and superconducting specimen at the lowest temperature of measurement (1.2 K), is plotted in Figure 21 as a function of ultrasonic frequency. In the absence of a quasiparticle density dependent dislocation attenuation, these attenuation values would be a measure of the total normal state electronic attenuations at 1.2 K as a function of frequency.

B. Data Analysis

The data analysis follows a method used by Mason (1966) and others. It is assumed that the measured attenuation (α_m) consists primarily of frequency and temperature dependent attenuations due to both free electrons (α_e) and dislocations (α_d). At the temperatures of these measurements, attenuation by other mechanisms will be either negligible
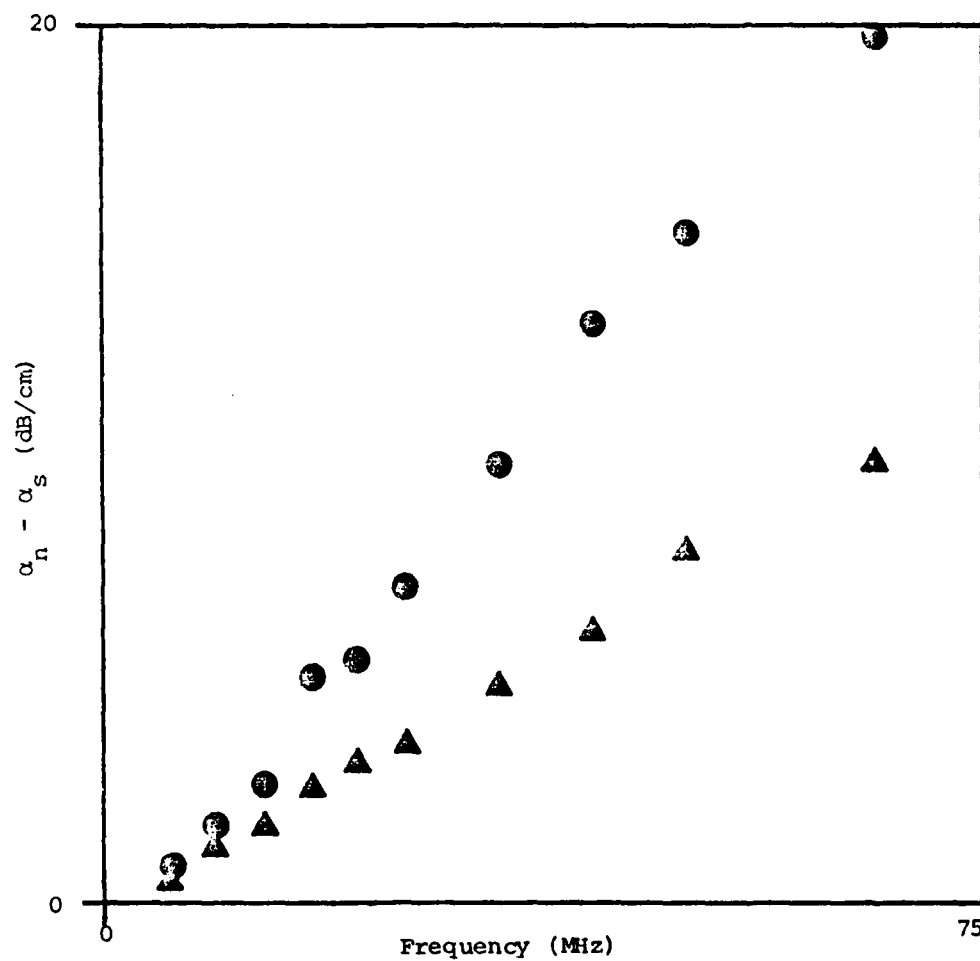
Figure 21.   Difference in normal and superconducting state attenuations at ~ 1.2 K as a function of frequency for the [100] specimen (●) and the [110] specimen (▲).

in magnitude (the case, for example, with anharmonic and phonon proc-
esses) or will be temperature independent (as with specimen to trans-
ducer band losses). These latter effects are accounted for by
including a residual system attenuation (α_r) in the list of contribu-
tions. The measured attenuation is therefore expressed as:

$$\alpha_m(\omega,T) = \alpha_e(\omega,T) + \alpha_d(\omega,T) + \alpha_r(\omega) \qquad (4.1)$$

which applies to both the normal and the superconducting state. This
expression is used to calculate the electronic components of the
attenuations:

$$\alpha_{es}(\omega,T) = \alpha_{ms}(\omega,T) - \alpha_{ds}(\omega,T) - \alpha_r(\omega)$$

and $\qquad (4.2)$

$$\alpha_{en}(\omega,T) = \alpha_{mn}(\omega,T) - \alpha_{dn}(\omega,T) - \alpha_r(\omega) \quad,$$

where the subscripts s and n indicate the superconducting and normal
states, respectively. Since the temperature dependence of the dis-
location damping arises solely through the varying density of non-
superconducting quasiparticles, normal state specimens will have
temperature independent dislocation attenuation. One can therefore
write

$$\alpha_{dn}(\omega,T) = \alpha_{dn}(\omega,T_c) = \alpha_{ds}(\omega,T_c) \qquad , \qquad (4.3)$$

where T_c is the superconducting transition temperature. With this
substitution, the subscript s on the dislocation attenuations can
therefore be dropped without ambiguity, giving for Equation (4.2):

$$\alpha_{es}(\omega,T) = \alpha_{ms}(\omega,T) - \alpha_d(\omega,T) - \alpha_r(\omega)$$

and   (4.4)

$$\alpha_{en}(\omega,T) = \alpha_{mn}(\omega,T) - \alpha_d(\omega,T_c) - \alpha_r(\omega) \quad .$$

If the value of dislocation and residual attenuations used for this calculation are correct, then the electronic attenuations thus obtained will be related by (Bardeen et al., 1957):

$$\frac{\alpha_{es}(\omega,T)}{\alpha_{en}(\omega,T)} = \frac{2}{(1 + e^{\varepsilon(T)/kT})} \equiv \beta(T) \quad ,$$ (4.5)

where $\varepsilon(T)$ is half the BCS superconducting energy gap. There is no closed analytical expression for $\varepsilon(T)$. BCS theory gives it in an integral form, and Muhlschlegel (1959) has tabulated it, but it is most convenient to use an approximate expression from Bliss and Rayne (1969) which is accurate to 0.5%:

$$\frac{\varepsilon(t)}{\varepsilon_0} = \left[\cos\left(\frac{1}{2}\pi t^2\right)\right]^{1/2} - 1.15 \times 10^{-3} \, e^{3.8t}\left[\sin 5.46(1-t)\right] \quad ,$$

(4.6)

where $t = T/T_c$ and, for indium, $\varepsilon_0 \simeq 1.85 \, kT_c$ and $T_c = 3.404$ K. Values for the dislocation attenuation are obtained by applying the conversion

$$\alpha(db/cm) = \frac{8.686}{2\pi} \frac{\omega}{v} \Delta$$ (4.7)

to the decrement equations taken from KGL theory. As shown in Chapter II, the dislocation decrement is predicted to be given by either

$$\Delta = \Delta_0 \int_0^\infty \frac{D\Omega \ x^5 \ dx}{\sinh \ (x) \ [(1-\Omega^2 x^2)^2 \ + \ D^2\Omega^2 x^4]} \tag{4.8}$$

or

$$\Delta = 2\Delta_0 \int_0^\infty \frac{D\Omega \ x^5 \ e^{-x} \ dx}{1 \ + (D\Omega)^2 x^4} \quad , \tag{4.9}$$

where $D = D_0 \beta(T) + \Omega/8$, $\Omega = \omega/\omega_0$, and D_0, ω_0 and Δ_0 are constants. As described earlier, these constants depend exclusively on crystal dislocation characteristics, and must be independent of the frequency and temperature of measurement. Since the value of these constants, as well as that of the residual attenuation, are not known, they are treated as variable parameters. A digital computer (Systems 85) is used to determine that set of values for the parameters which results in a best fit of the equality

$$\frac{\alpha_{ms}(\omega,T) \ - \ \alpha_d(\omega,T) \ - \ \alpha_r(\omega)}{\alpha_{mn}(\omega,T) \ - \ \alpha_d(\omega,T_c) \ - \ \alpha_r(\omega)} = \beta(T) \tag{4.10}$$

over the temperature range of interest. If there is a set of parameter values for which this equality holds, these are taken to be the correct values of Δ_0, ω_0 and D_0 as specified by the KGL theory.

The problem of determining the best fitting values of Δ_0, ω_0 and D_0 [i.e., the simultaneous solution, for a large number of temperature dependent data points, of Equations (4.10) and either (4.8) or (4.9)] does

not lend itself to an analytical solution. A computer algorithm which
was developed to resolve this difficulty allows a systematic search
of the possible parameter values. A reasonable domain for each con-
stant is identified and then divided into a large number of intervals.
For each possible combination of the parameter values thus obtained,
the dislocation attenuation is calculated from the KGL theory and the
subsequent goodness of fit for Equation (4.10) is determined. Parameter
combinations which allow a good correspondence between theory and data
are identified in this way. Despite optimization of this algorithm,
approximately fifty hours of computer time is required to extract
from one data set reliable best fit values for Δ_0, ω_0 and D_0.

C. Results

Attracted by its relative simplicity (as compared to the exact
expression) and following the example of Granato and Lücke, the first
attempts at analysis of the data employed the approximated form of the
KGL theory [Equation (4.9)]. Working with a single data set, it
was found that there is indeed a triple of values for the parameters
Δ_0, ω_0 and D_0 which, through Equation (4.9), provides a correction that
brings the data into good agreement with the BCS prediction. A
comparison of the corrected and uncorrected data with the BCS curve
is shown in Figure 22. In this case, the data was recorded using
10 MHz ultrasound and the best fitting values of the parameters were
$\Delta_0 = 0.0053$, $\omega_0 = 12.6$ MHz, and $D_0 = 0.50$. This result is similar
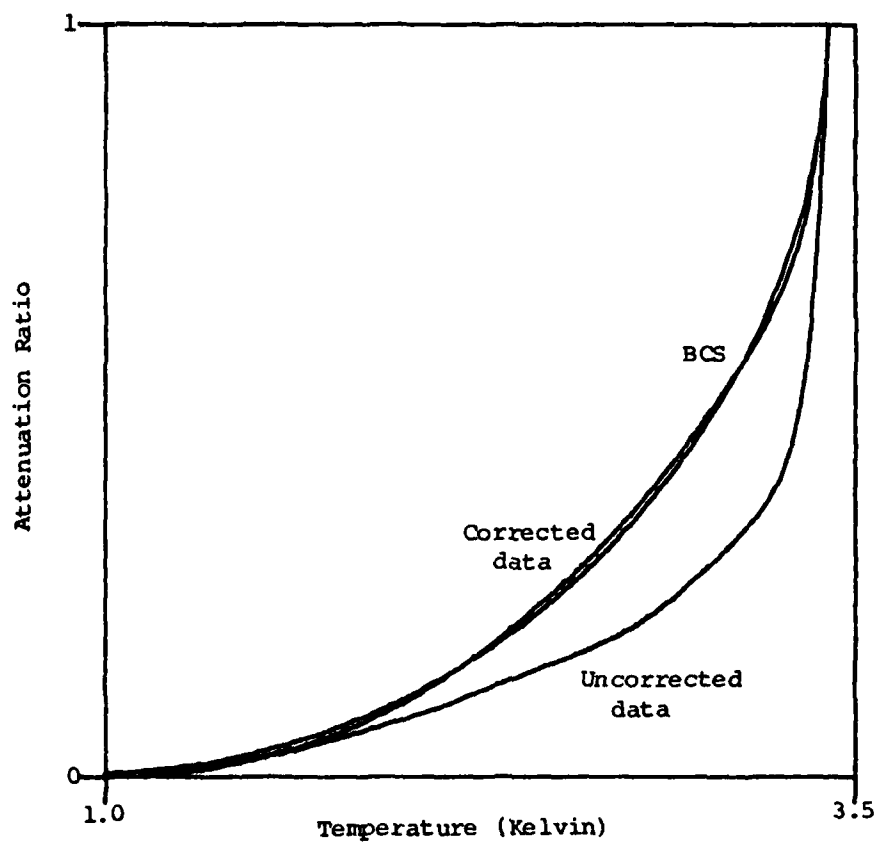to that of Mason (1966) for attenuations in tin. When the corrections

Figure 22. Comparison of corrected and uncorrected data to
BCS-like behavior using the approximated theory.

determined by these parameter values were applied to data taken at other ultrasonic frequencies; however, little or no improvement in the correlation of theory and data were obtained. This is demonstrated in Figure 23 with data taken at 6 and 50 MHz. Mason did not work with a sufficiently large range of frequencies to observe this inconsistency, and hence, he has concluded his form of the approximated theory to be valid.

It has been determined that, for any set of the data, there is some triple of parameter values by which a correction equivalent to that shown in Figure 22 can be obtained. These values, however, differ greatly for data sets taken at different ultrasonic frequencies, thus contradicting the invariant nature of the constants Δ_0, ω_0 and D_0. In addition, it was found that for each best fitting triple of parameters, the ratio ω/ω_0 is approximately equal to unity, this violating the assumption $(\omega/\omega_0)^2 \ll 1$ which was fundamental to the approximated theory. For these reasons, the approximated KGL theory [Equation (4.9)] was determined to be inapplicable to the analysis of this data.

Following rejection of the approximate form of the KGL theory, the analysis was repeated using the exact expression of the theory, Equation (4.8). The results of this analysis showed no significant change from those obtained formerly. Again, it was determined that for any set of the data, there is some triple of values for the constants Δ_0, ω_0 and D_0 through which the KGL theory provides just the correction necessary to explain the deviation of that data from the BCS prediction. A typical matching of the corrected data to the
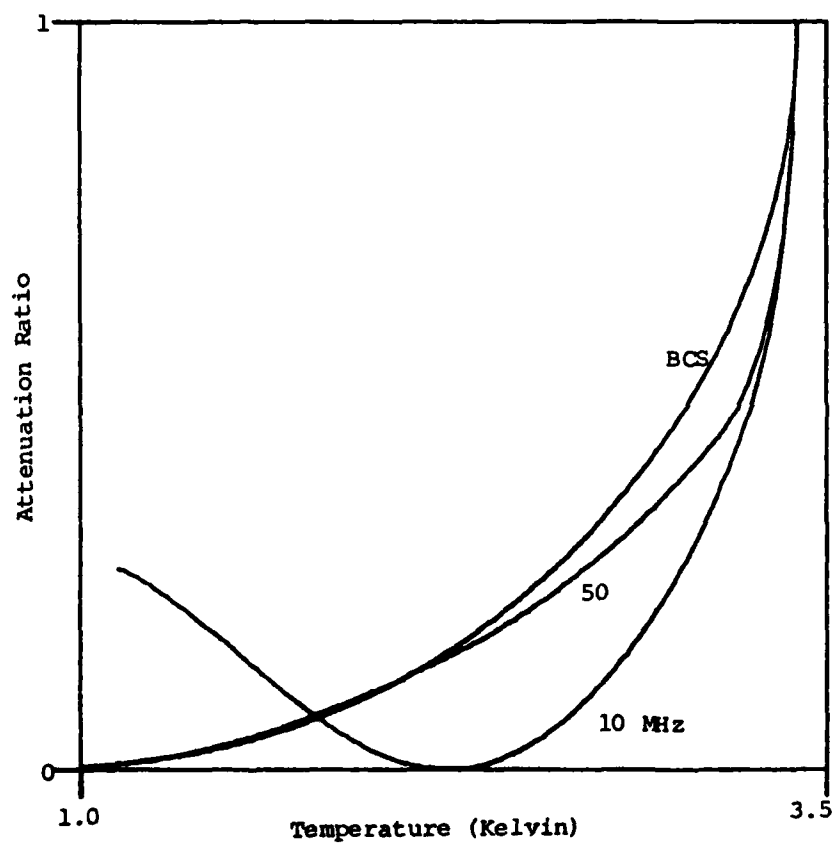
Figure 23. Result of applying 10 MHz data corrections to
6 and 50 MHz data.

BCS relation is shown in Figure 24. The constants determined from different data sets, however, continue to fluctuate widely, showing a dependence on ultrasonic frequency that is not consistent with the invariant nature of these parameters.

Precise values for the three constants are not acquired through this analysis. It has been observed that parameter values varying by as much as 25% from the best fitting values may also give an acceptably good fit to the BCS relation. The tolerable variations for the three parameters are interdependant, however, and a good fit can be maintained only if the values are changed in a particular way. (Generally, a decrease in ω_0 must be accompanied by increases in Δ_0 and D_0.) This latitude in the best fitting values is a result of fluctuations in the data and the slowly varying nature of the KGL equations. The considerable tolerance in parameter values is not sufficient to allow a triple of numbers which will suitably correct more than a single frequency of data. There is no set of values for the constants which allows the KGL theory to account for the deviations in multifrequency data.

The uncertainty in the best fit value for the parameters Δ_0, ω_0, and D_0 makes it difficult to describe the manner in which they vary with the ultrasonic frequency. At best, one can say that the values of the latter two appear to increase linearly with frequency (the proportionality constants are $\omega_0/\omega \sim 1.7$ and $D_0/\omega \sim 1.9$) while Δ_0 remains constant (~ 0.005). No physical significance can be ascribed to this behavior. This discussion only serves to emphasize
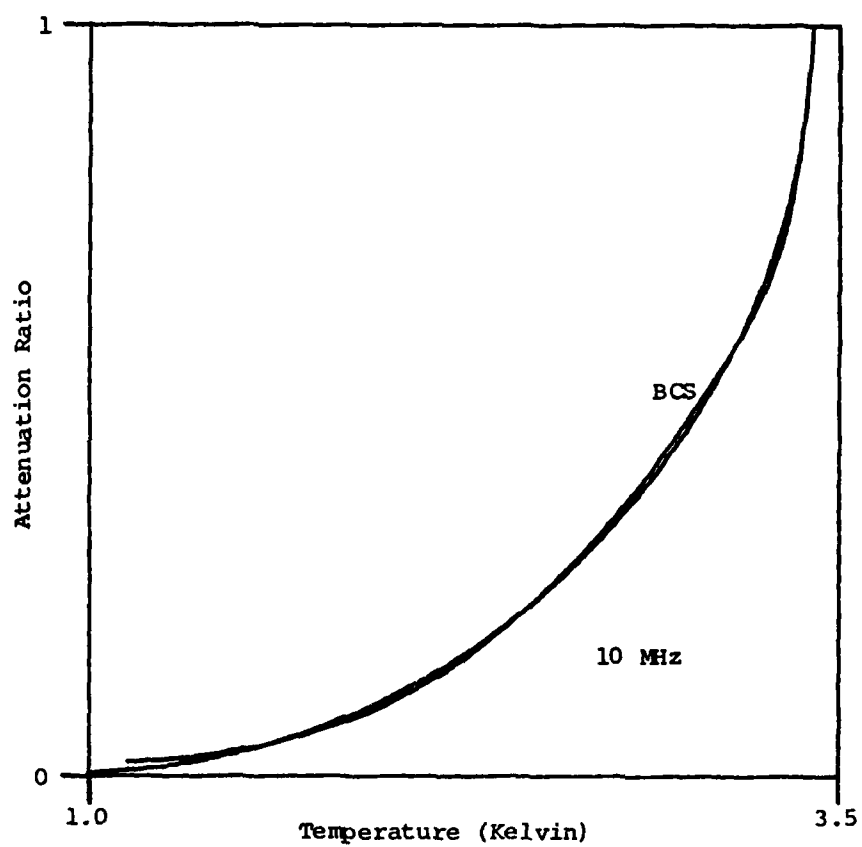
Figure 24.   Comparison of corrected data to BCS-like behavior
using the exact theory.

the manner in which failure of the KGL theory has been recognized. The
values given above pertain to data measured in the specimen for which
sound propagation was along the [100] crystal axis. Otherwise, the
experimental results described apply to the data collected in both this
specimen and the one with the [110] orientation.

The theory of ultrasonic attenuation by dislocations formulated
by Granato and Lücke is unable to account for the attenuation,
additional to that caused by conduction electrons, which has been ob-
served in superconducting indium. It is therefore necessary to conclude
that the KGL theory is inapplicable to the situation of this experiment,
i.e., to indium at low temperatures.

D. Empirical Description of the Data

The contribution of dislocations to the net ultrasonic attenuation
could be determined from the experimental data in the following way.
The measured relative attenuation is considered to vary as the sum
of four terms:

1) $\alpha_e(\omega,T)$ - The electronic attenuation which is frequency
   and temperature dependent.

2) $\alpha_d(\omega,T)$ - The dislocation attenuation which is also
   frequency and temperature dependent.

3) $\rho(\omega)$ - A residual attenuation, inherent in the ultrasonic
   system, which may vary with frequency.

4) $\sigma(\omega)$ - An undetermined shift in the attenuation calibration
   associated with the arbritrary assignment of a level of zero
   decibels to the maximum observed echo signal.

The measured attenuation is then expressed as:

$$\alpha_m(\omega,T) = \alpha_e(\omega,T) + \alpha_d(\omega,T) + \rho(\omega) + \sigma(\omega) \quad . \tag{4.11}$$

This applies to both the superconducting state and normal state data, so Equation (4.11) can be written as:

$$\alpha_{ms}(\omega,T) = \alpha_{es}(\omega,T) + \alpha_{ds}(\omega,T) + \rho(\omega) + \sigma(\omega) \tag{4.12}$$

and

$$\alpha_{mn}(\omega,T) = \alpha_{en}(\omega,T) + \alpha_{dn}(\omega,T) + \rho(\omega) + \sigma(\omega) \quad . \tag{4.13}$$

As discussed earlier, the normal state dislocation attenuation is expected to be temperature independent and equal to the superconducting state attenuation at the superconducting transition temperature. That is:

$$\alpha_{dn}(\omega,T) = \alpha_{dn}(\omega,T_c) = \alpha_{ds}(\omega,T_c) \quad . \tag{4.14}$$

Again, the subscripts n and s on the dislocation attenuations can be dropped without ambiguity. The electronic attenuations in the superconducting and normal states are related by:

$$\frac{\alpha_{es}(\omega,T)}{\alpha_{en}(\omega,T)} = \beta(T) \quad , \tag{4.15}$$

where $\beta(T)$ is the well known BCS relation defined in Equation (4.5).

Equations (4.12) to (4.15) can be combined to give as an expression for the dislocation attenuation:

$$\alpha_d(\omega,T) = \left[\alpha_{ms}(\omega,T) - \beta(T)\alpha_{mn}(\omega,T)\right] - \left[1 - \beta(T)\right]\left[\rho(\omega) + \sigma(\omega)\right] + \beta(T)\alpha_d(\omega,T_c) \quad .$$

$$\tag{4.16}$$

At the lowest temperature of measurement (T_0), the ultrasonic signal measured in the superconducting specimen is a maximum, and Equation (4.12) becomes:

$$\alpha_{ms}(\omega,T_0) = \alpha_{es}(\omega,T_0) + \alpha_d(\omega,T_0) + \rho(\omega) + \sigma(\omega) = 0 \quad , \tag{4.17}$$

so that

$$\rho(\omega) + \sigma(\omega) = -\left[\alpha_{es}(\omega,T_0) + \alpha_d(\omega,T_0)\right] \quad . \tag{4.18}$$

Making this substitution into Equation (4.16) then gives:

$$\alpha_d(\omega,T) = \left[\alpha_{ms}(\omega,T) - \beta(T)\alpha_{mn}(\omega,T)\right] + \left[1-\beta(T)\right]\left[\alpha_{es}(\omega,T_0) + \alpha_d(\omega,T_0)\right]$$

$$+ \beta(T)\alpha_d(\omega,T_c) \quad . \tag{4.19}$$

In order to use this expression to calculate the dislocation attenuation, two absolute attenuation values, in addition to the measured relative attenuations (the α_m), must be known. One, $\alpha_{es}(\omega,T_0) + \alpha_d(\omega,T_0)$ is the sum of the electronic and dislocation attenuations at the lowest temperature of superconducting state measurement. This is determined from secondary data recording the rate of exponential decrease of the ultrasonic echo amplitudes at that particular frequency and temperature. These measurements are subject to errors [such as signal losses due to non-parallelness of the specimen surfaces, diffraction of the ultrasonic waves, and transducer bond losses (Morse, 1959)] which do not affect single-echo measurements of relative attenuation. Values of absolute attenuation obtained in this

way, therefore, can only serve to indicate the general variation of the data.

The other value which must be known, $\alpha_d(\omega, T_c)$, is the dislocation attenuation at the superconducting transition temperature. This cannot be determined with the experimental apparatus available, which makes no provision for distinguishing explicitly between the contributions of electrons and of dislocations to the net attenuation. To do so, a system like that used by Thompson and Pare (1966) would be required. In their experiment, the dislocation attenuation is directly indicated by the change in net attenuation which results from extensive neutron bombardment of the specimen; the neutron damage introducing pinning centers which eventually lock the dislocations into fixed positions. Lacking the value of $\alpha_d(\omega, T_c)$ prohibits an empirical description of the dislocation data. The available data may, however, suggest the nature of the temperature and frequency dependence of the dislocation attenuation.

The second and third terms on the right side of Equation (4.19) are already separated into factors which depend uniquely on temperature or on frequency. The first term of that equation is found empirically to also have separable temperature and frequency dependencies. Its normalized temperature dependence is plotted in Figure 25, and the frequency dependent amplitude of that curve is included in Figure 26. The frequency variation of the second term, also plotted in Figure 26, is equal to that of the first, within experimental error. If the
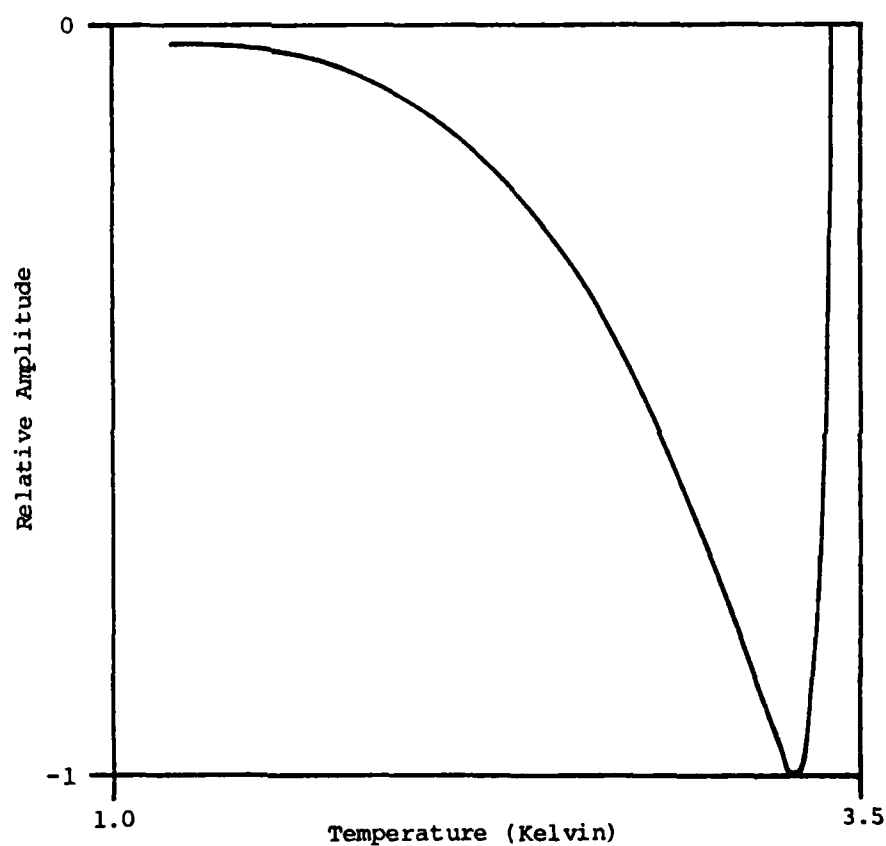
Figure 25.   Normalized temperature dependence of $\alpha_{ms}(\omega,T)$ – $\beta(T)\alpha_{mn}(\omega,T)$.
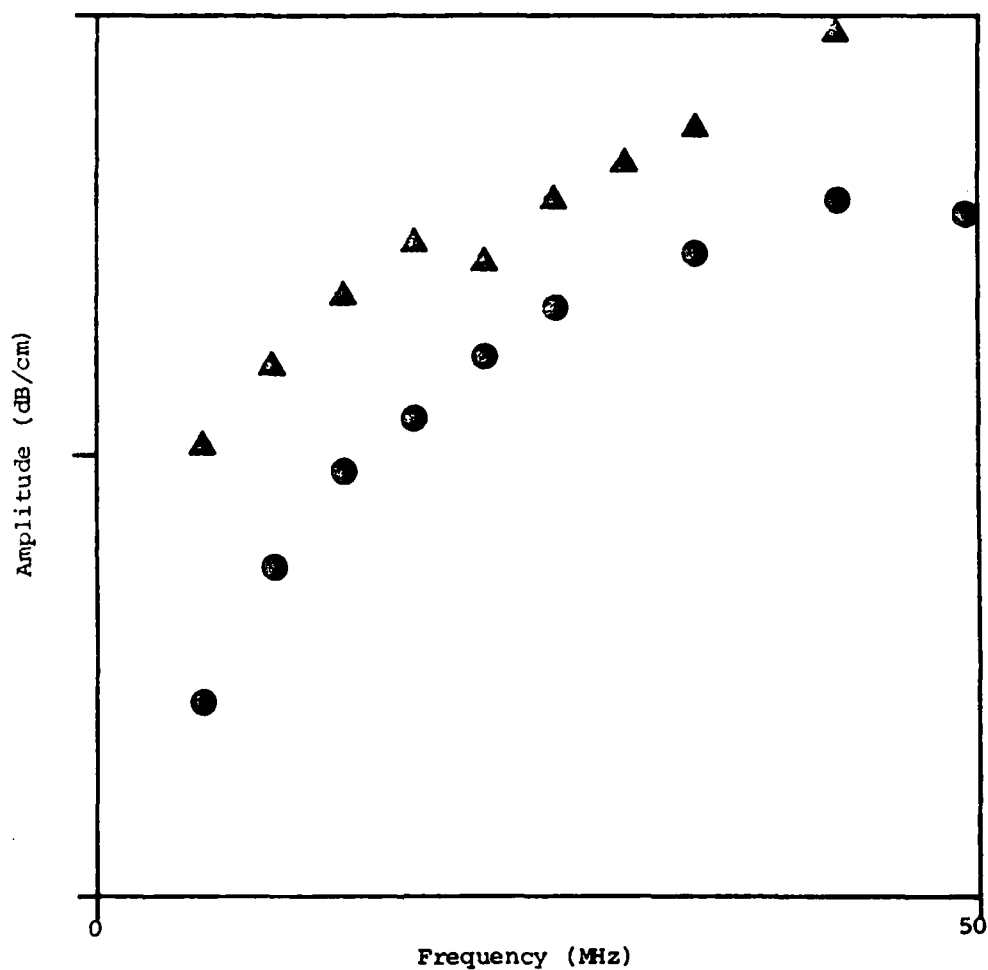
Figure 26. Frequency dependencies of $[\alpha_{ms}(\omega,T) - \beta(T)\alpha_{mp}(\omega,T)]$ ($\bullet$) and $[\alpha_{es}(\omega,T_0) + \alpha_d(\omega,T_0)]$ ($\blacktriangle$) for the [100] specimen.

third term were shown to have this same frequency dependence, then the
dislocation attenuation itself could be neatly expressed as the product
of separable temperature and frequency factors.

The fact that the first term in Equation (4.19) is negative has no
real significance, since these terms do not have any physical meaning
if taken individually. It is necessary, of course, that the sum of the
terms be always positive since a negative attenuation would indicate
the spontaneous generation of ultrasound. The second and third terms
of Equation (4.19) are everywhere positive. The magnitude of the
second, which is known, is not always sufficient to balance the nega-
tive going first term. It is thus possible to determine a minimum
value for $\alpha_d(\omega, T_c)$ which makes the attenuation invariably positive.
A lower limit on $\alpha_d(\omega, T_c)$ derived in this way can only serve as an
indication of the nontrivial contribution of dislocations to the
normal state attenuation of the specimen. For example, the data
measured at 10 MHz in the [100] specimen indicates a minimum normal
state dislocation attenuation of 0.1 dB per cm. The actual value
of the attenuation can only be described as greater than this.

The results described above pertain to data collected in that
crystal which had its [100] axis parallel to the direction of sonic
propagation. Analysis of data taken with the second specimen, for
which propagation was along the [110] axis, yields results consistent
with those already described. In this case, calculation of the
individual terms in Equation (4.19) again shows the difference

$\alpha_{ms}(\omega,T)-\beta(T)\alpha_{mn}(\omega,T)$ to have the temperature dependence plotted in Figure 25. As expected, the amplitude of this term, as well as that of the measurable absolute attenuation $\alpha_{es}(\omega,T_0) + \alpha_d(\omega,T_0)$ are found to be directionally dependent. These amplitudes, for the second specimen, are plotted in Figure 27.
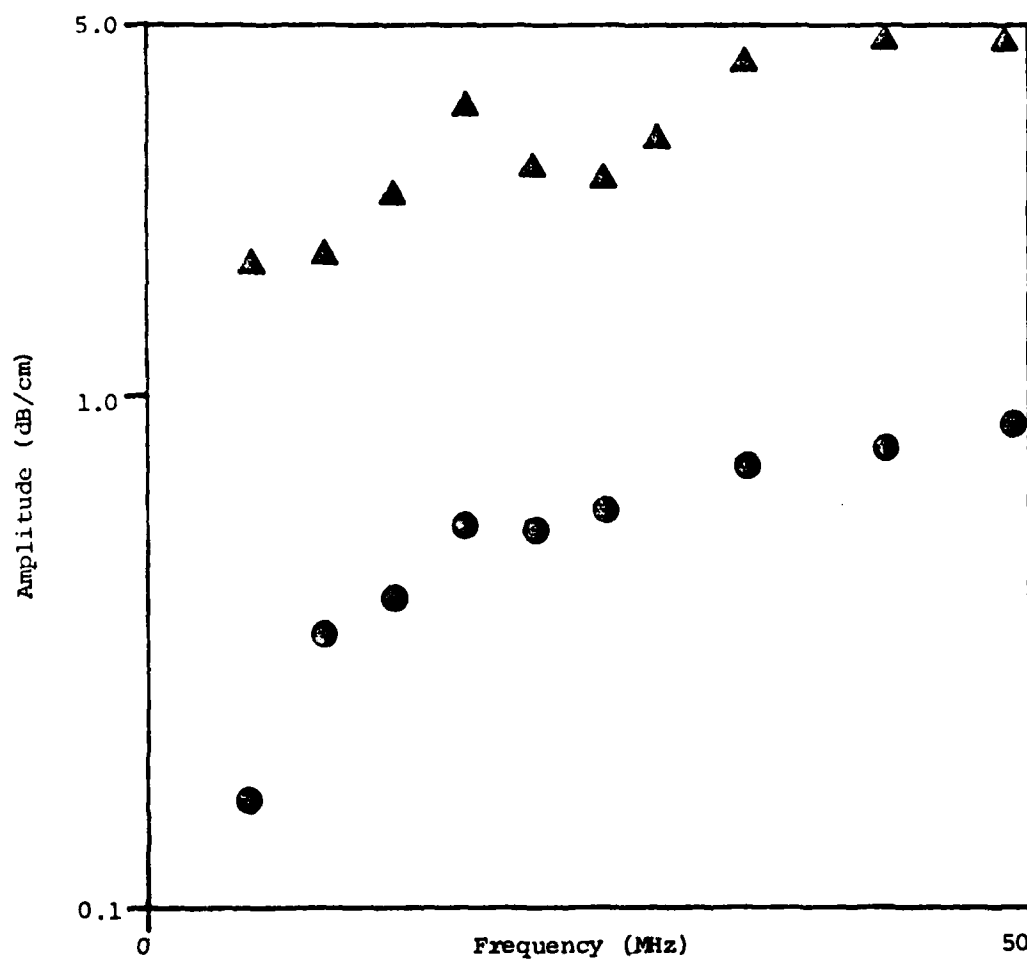
Figure 27. Frequency dependencies of $[\alpha_{ms}(\omega,T) - \beta(T)\alpha_{mn}(\omega,T)]$ ($\bullet$) and $[\alpha_{es}(\omega,T_0) + \alpha_d(\omega,T_0)]$ ($\blacktriangle$) for the [110] specimen.

V. CONCLUSION

The ultrasonic attenuation in a superconducting material is expected to vary with temperature according to the BCS relation:

$$\frac{\alpha_{es}(T)}{\alpha_{en}(T)} = \frac{2}{1 + e^{\epsilon(T)/kT}} \quad ,$$

where $\epsilon(T)$ is half the BCS superconducting energy gap. There are cases, however, in which the measured attenuations are seen to deviate from this behavior. This is generally attributed to an interaction between the sound waves and crystal dislocations, one mechanism for which is given by the theory of Koehler (1952) and Granato and Lücke (1956). This theory has found considerable success in describing a variety of dislocation phenomenon, and was applied to the superconduction anomaly by several authors, Mason (1966) most notably. The research described in this thesis has expanded the investigation of this anomaly by recording temperature dependent attenuations for a wide range of ultrasonic frequencies. Formerly reported data consist mostly of single frequency measurements. By analysis of this expansive data, it has been shown conclusively that the KGL theory is not able to explain the deviation in indium of measured attenuations from BCS-like behavior. It has thus been determined that the KGL theory is inapplicable to the case of low temperature indium. Earlier work which appears to contradict this result has been shown to be an insufficient test of the theory.

The failure of the otherwise successful KGL model to describe the superconducting phenomenon may be attributed to either of two apparent weaknesses in the theory. First is the possibility that, at very low temperatures, the crystal through which the dislocation moves can no longer be viewed as a continuum, as Granato and Lücke have assumed. The possible effect of crystal structure on a dislocations shape and motion are reviewed by Seeger and Schiller (1966). Most work on this topic has been concerned with phonon-dislocation interactions in non-conducting crystals (e.g., Seeger and Engelke, 1968). No conclusive theory relating crystal structure to dislocation dynamics for a low temperature metal has been published. The other possible fault lies in the expression [Equation (2.4)] used to calculate the electronic component of the dislocation drag. The relevant drag coefficient has not been measured directly, so that while this expression is generally believed to be accurate, the discussion of Huffmann and Loaut (1970), for instance, shows that a reasonable doubt does exist. Considering these weaknesses, it is not very surprising that the KGL model does not explain the attenuation anomaly observed in super-conducting indium. The need for further theoretical investigation of this topic is now apparent.

This work has exhausted the possibilities for experimental study of the phenomenon. Without a more reliable theory by which to evaluate the data, no practical further effort can be conceived.

REFERENCES

Bardeen, J., Cooper, L. N., and Schrieffer, J. R. (1957), Phys. Rev. 108, 1175.

Binnie, D. E. (1971), Ph.D. Thesis, The Pennsylvania State University.

Bliss, E. S., and Rayne, J. A. (1969), Phys. Rev. 177, 673.

Bömmel, H. E. (1954), Phys. Rev. 96, 220.

Brailsford, A. D. (1966), Phys. Rev. 142, 388.

Brailsford, A. D. (1969), Phys. Rev. 186, 959.

Burgers, J. M. (1939), Proc. Koninkl. Ned. Akad. Wetenschap. 42, 293; 42, 378.

Cisney, E. A. (1959), Trans. Met. Soc. AIME 215, 538.

Cottrell, A. H. (1948), Rept. Conf. Strength Solids, (1948), p. 30, Phys. Soc., London.

Garber, J. A., and Granata, A. V. (1970), J. Phys. Chem. Solids 31, 1863.

Granato, A. and Lücke, K. (1956), J. Appl. Phys. 27, 583.

Huffman, G. P. and Louat, N. (1970), Phys. Rev. Lett. 24, 1055.

Koehler, J. S. (1952), "Imperfections in Nearly Perfect Crystals," Chapter 7, Wiley, New York.

Leibfried, G. (1950), Z. Physik 127, 344.

Love, R. E. and Shaw, R. W. (1964), Rev. Mod. Phys. 34, 260.

Mackinnon, L. (1955), Phys. Rev. 98, 1181.

Mason, W. P. (1958), "Physical Acoustics and The Properties of Solids," Chapter 9, Van Nostrand, Princeton, New Jersey.

Mason, W. P. (1966), "Physical Acoustics," Vol. IV A, Chap. 8, (Warren P. Mason, ed.), Academic Press, New York.

Merkulov, L. G. and Yakovlev, L. A. (1960), Sov. Phys.-Acoustics $\underline{6}$, 239.

Morse, R. W. and Bohm, H. V. (1957), Phys. Rev. $\underline{108}$, 1094.

Morse, R. W. (1959), Prog. Cryog. $\underline{1}$, 219.

Muhlschlegel, B. (1959), Z. Physik $\underline{155}$, 313.

Nabarrow, F. R. N. (1947), Proc. Phys. Soc. (London) $\underline{59}$, 256.

Oen, O. S., Holmes, D. K., and Robinson, M. T. (1960), Solid State
    Division Annual Report, August 31, 1960, U.S.A.E.C. Report
    ORNL-3017, p. 3.

Peach, M. and Koehler, J. S. (1950), Phys. Rev. $\underline{80}$, 436.

Pippard, A. B. (1955), Phil. Mag. $\underline{46}$, 1104.

Preuss, E., Krahl-Urban, B., Butz, R. (1974), "Laue Atlas," Wiley,
    New York.

Rayleigh, Lord (1894), "Theory of Sound," Chap. 6, (reprinted by Dover
    Publications, New York).

Read, M. P. and Brailsford, A. D. (1974), J. Appl. Phys. $\underline{45}$, 3351.

Seeger, A. and Engelke, H. (1968), "Dislocation Dynamics," p. 623, (Alan
    R. Rosenfeld, ed.), McGraw-Hill, New York.

Seeger, A. and Schiller, P. (1966), "Physical Acoustics," Vol. III A,
    Chap. 8 (Warren P. Mason, ed.), Academic Press, New York.

Thompson, D. O. and Holmes, D. K. (1956), J. Appl. Phys. $\underline{27}$, 713.

Thompson, D. O. and Pare, V. K. (1966), "Physical Acoustics," Vol.
    III A, Chap. 7, (Warren P. Mason, ed.), Academic Press, New York.

Tittmann, B. R. and Bommel, H. E. (1966), Phys. Rev. $\underline{151}$, 178.

Tittmann, B. R. (1975), "Internal Friction in Crystaline Solids,"
    Vol. I, p. 52, (D. Lenze and K. Lucke, ed.), Springer-Verlag,
    New York.

Wood, E. A. (1963), "Crystal Orientation Manual," Columbia University
    Press, New York.

APPENDIX A

Expressions for the dislocation displacement, $\xi(x,y,t)$, and the
dislocation attenuation, $\alpha(x,y,t)$, are obtained by the simultaneous
solution of

$$A \frac{\partial^2}{\partial t^2} \xi + B \frac{\partial}{\partial t} \xi - C \frac{\partial^2}{\partial y^2} \xi = b\sigma \quad , \tag{A.1}$$

$$\sigma = \sigma_0 \, e^{-\alpha x} \, \cos\theta \quad ; \quad \theta = \omega t - 2\pi x/\lambda \tag{A.2}$$

and

$$\frac{\partial^2}{\partial x^2} \sigma - \frac{\rho}{G} \frac{\partial^2}{\partial t^2} \sigma = \rho b \frac{\partial^2}{\partial t^2} \int_0^{\ell} \xi \, dy \tag{A.3}$$

subject to the constraint $\xi(x,o,t) = \xi(x,\ell,t) = 0$.

A.   Dislocation Displacement

A function which is defined on the interval $0 \leq y \leq \ell$ may be
expressed as a Fourier sine series. If the dislocation displacement is
described in this way, only the odd terms in the series need to be
considered since even terms represent an asymmetric displacement for
which the net strain, and hence, the contribution to the attenuation,
is zero. The dislocation displacement is therefore written as:

$$\xi(x,y,t) = \sum_{n=o}^{\infty} T_n(x,t) \, \sin\phi_n y; \quad \phi_n = \frac{(2n+1)\pi}{\ell} \quad . \tag{A.4}$$

Using the standard notation of dots and primes to represent partial
derivatives with respect to t and y, respectively, one calculates

from Equation (A.4):

$$\dot{\xi} = \sum_{n=o}^{\infty} \dot{T}_n \sin\phi_n y \quad , \tag{A.5a}$$

$$\ddot{\xi} = \sum_{n=o}^{\infty} \ddot{T}_n \sin\phi_n y \tag{A.5b}$$

and

$$\xi'' = - \sum_{n=o}^{\infty} T_n \phi_n^2 \sin\phi_n y \quad . \tag{A.5c}$$

A useful identity is:

$$1 = \frac{4}{\pi} \sum_{n=o}^{\infty} \frac{1}{(2n+1)} \sin\phi_n y \quad ; \quad 0 \leq y \leq \ell \quad . \tag{A.6}$$

Substitution of Equations (A.2),(A.5),and (A.6) into Equation (A.1) leads to

$$\sum_{n=o}^{\infty} (A \ddot{T}_n + B \dot{T}_n + C\phi_n^2 T_n)\sin\phi_n y = \sum_{n=o}^{\infty} D_n \cos\theta \sin\phi_n y \quad , \tag{A.7}$$

where

$$D_n(x) = \frac{4b\sigma_0 \ e^{-\alpha x}}{(2n+1)\pi} \quad .$$

Equating the coefficients of the $\sin\phi_n y$ gives:

$$A \ddot{T}_n + \dot{B} T_n + C\phi_n^2 T_n = D_n \cos\theta \tag{A.8}$$

for each n. This equation has a solution of the form:

$$T_n(x,t) = E(x) \cos\theta(t) + F(x) \sin\theta(t) \tag{A.9a}$$

for which

$$\dot{T}_n = -\omega \, E \, \sin\theta + \omega \, F \, \cos\theta \tag{A.9b}$$

and

$$\ddot{T}_n = -\omega^2 \, E \, \cos\theta - \omega^2 \, F \, \sin\theta \quad . \tag{A.9c}$$

Substitution of Equations (A.9) into Equation (A.8) and equating the coefficients of $\cos\theta$ and of $\sin\theta$ gives

$$-A \, \omega^2 \, E + B \, \omega \, F + C\phi_n^2 \, E = D_n \tag{A.10a}$$

and

$$-A \, \omega^2 \, F - B \, \omega \, E + C\phi_n^2 \, F = 0 \quad . \tag{A.10b}$$

From this, the factors $E(x)$ and $F(x)$ are determined to be:

$$E = \frac{-D_n(A\omega^2 - C\phi_n^2)}{B^2\omega^2 + (A\omega^2 - C\phi_n^2)^2} \tag{A.11a}$$

and

$$F = \frac{B\omega D_n}{B^2\omega^2 + (A\omega^2 - C\phi_n^2)^2} \quad . \tag{A.11b}$$

The dislocation displacement, determined by Equations (A.4), (A.9a), and (A.11) is therefore given by:

$$\xi(x,y,t) = \sum_{n=o}^{\infty} \left[\frac{-D_n(A\omega^2 - C\phi_n^2)}{B^2\omega^2 + (A\omega^2 - C\phi_n^2)^2} \cos\theta + \frac{B\omega D_n}{B^2\omega^2 + (A\omega^2 - C\phi_n^2)^2} \sin\theta \right] \sin\phi_n y \ ,$$

$$\tag{A.12}$$

where

$$D_n = \frac{4b\sigma_0\ e^{-\alpha x}}{(2n+1)\pi} \quad , \tag{A.13a}$$

$$\phi_n = \frac{(2n+1)\pi}{\ell} \tag{A.13b}$$

and

$$\theta = \omega t - 2\pi x/\lambda \quad . \tag{A.13c}$$

This expression will bear considerable simplification. By using the identity

$$E\cos\theta + F\sin\theta = (E^2 + F^2)^{1/2}\cos(\theta-\delta) \quad , \tag{A.14a}$$

where

$$\delta = \arctan\ (F/E) \ , \tag{A.14b}$$

the dislocation displacement may also be written as:

$$\xi(x,y,t) = \sum_{n=o}^{\infty} \frac{D_n}{\left[B^2\omega^2 + (A\omega^2 - C\phi_n^2)^2\right]^{1/2}}\ \cos(\theta-\delta_n)\sin\phi_n y \quad , \tag{A.15a}$$

where D_n, ϕ_n, and θ are as defined above and

$$\delta_n = \arctan\left[\frac{B\omega}{C\phi_n^2 - A\omega^2}\right] \quad . \tag{A.15b}$$

Finally, by substituting for D_n and ϕ_n, and defining the constant

$$\omega_0 = \frac{\pi}{\ell} \left(\frac{C}{A}\right)^{1/2} \quad , \tag{A.16a}$$

one writes the dislocation displacement as:

$$\xi(x,y,t) = \frac{4b\sigma_0}{A\pi} e^{-\alpha x} \sum_{n=0}^{\infty} \frac{1}{(2n+1)} \sin \frac{(2n+1)\pi y}{\ell}$$

$$\times \frac{e^{i(\omega t - 2\pi x/\lambda - \delta_n)}}{\left[\left[(2n+1)^2 \omega_0^2 - \omega^2\right]^2 + (B/A)^2 \omega^2\right]^{1/2}} \tag{A.16b}$$

with

$$\delta_n = \arctan \left[\frac{(B/A)\omega}{(2n+1)^2 \omega_0^2 - \omega^2}\right] \quad . \tag{A.16c}$$

B. Dislocation Attenuation

If the dislocation displacement [Equation (A.12)] is expressed as:

$$\xi = \sum_{n=0}^{\infty} (E \cos\theta + F \sin\theta) \sin\phi_n y \quad , \tag{A.17}$$

then one calculates

$$\int_0^{\ell} \xi \, dy = \sum_{n=0}^{\infty} (E \cos\theta + F \sin\theta) \int_0^{\ell} \sin\phi_n y \quad .$$

Recall that $\phi_n = (2n+1)\pi/\ell$, so that

$$\int_0^\ell \sin\phi_n y = \frac{2\ell}{(2n+1)\pi}$$

and

$$\int_0^\ell \xi \, dy = \sum_{n=o}^{\infty} \frac{2\ell}{(2n+1)\pi} (E \cos\theta + F \sin\theta) \quad . \tag{A.18}$$

From this, one calculates

$$\frac{\partial^2}{\partial t^2}\int_0^\ell \xi \, dy = \sum_{n=o}^{\infty} \frac{-2\ell\omega^2}{(2n+1)\pi} (E \cos\theta + F \sin\theta) \tag{A.19}$$

which, by the definitions of E and F [Equations (A.11)] is equivalent to:

$$\frac{\partial^2}{\partial t^2}\int_0^\ell \xi \, dy = \frac{2\ell\omega^2}{\pi} \sum_{n=o}^{\infty} \frac{1}{(2n+1)}$$

$$\times \left[\frac{D_n(A\omega^2 - C\phi_n^2)}{B^2\omega^2 + (A\omega^2 - C\phi_n^2)^2} \cos\theta - \frac{D_n B\omega}{B^2\omega^2 + (A\omega^2 - C\phi_n^2)^2} \sin\theta \right] \quad .$$

$$\tag{A.20}$$

From Equation (A.2), one obtains:

$$\frac{\partial^2}{\partial t^2} \sigma = -\omega^2\sigma_0 \, e^{-\alpha x} \cos\theta \tag{A.21a}$$

and

$$\frac{\partial^2}{\partial x^2}\,\sigma = \sigma_0\,e^{-\alpha x}\left[\left(\alpha^2 - \frac{4\,\pi^2}{\lambda^2}\right)\cos\theta - \frac{4\pi\alpha}{\lambda}\,\sin\theta\right]\quad. \tag{A.21b}$$

Substitution of Equation (A.20) and (A.21) into Equation (A.3), and equating the coefficients of $\sin\theta$:

$$\sigma_0\,e^{-\alpha x}\,\frac{4\pi\alpha}{\lambda} = \frac{2\rho b \ell \omega^2}{\pi}\sum_{n=0}^{\infty}\frac{1}{(2n+1)}\,\frac{D_n B\omega}{B^2\omega^2 + (A\omega^2 - C\phi_n^2)^2}\quad. \tag{A.22}$$

Substituting for D_n from Equation (13.a) and solving for the dislocation attenuation, α, gives:

$$\alpha = \frac{2\rho b^2 \ell \lambda \omega^2}{\pi^3}\sum_{n=0}^{\infty}\frac{1}{(2n+1)^2}\,\frac{B\omega}{B^2\omega^2 + (A\omega^2 - C\phi_n^2)^2}\quad. \tag{A.23}$$

Using the relations

$$\omega\lambda = 2\,v\quad,$$

$$v^2 = G/\rho$$

and

$$C = \frac{1}{2}\,Gb^2\quad,$$

Equation (A.23) reduces to:

$$\alpha = \frac{8\omega\ell^3}{v\pi^4}\sum_{n=0}^{\infty}\frac{1}{(2n+1)^2}\,\frac{D\Omega}{\left[(2n+1)^2 - \Omega^2\right]^2 + D^2\,\Omega^2}\quad, \tag{A.24a}$$

where

$$D = \frac{(B/A)}{\omega_0} \quad , \tag{A.24b}$$

$$\Omega = \frac{\omega}{\omega_0} \tag{A.24c}$$

and

$$\omega_0 = \frac{\pi}{\ell} \left(\frac{C}{A}\right)^{1/2} \quad . \tag{A.24d}$$

APPENDIX B

The decrement that results from an assembly of dislocations is obtained by solving

$$\Delta = \int_0^\infty \Delta_\ell \; N(\ell) \; d\ell \quad , \tag{B.1}$$

where $N(\ell) \cdot d\ell$, the number of dislocations having loop lengths between ℓ and $\ell + d\ell$, is given by:

$$N(\ell) = \frac{\Lambda}{L^2} \, e^{-\ell/L} \tag{B.2}$$

and Δ_ℓ, the decrement from a single loop of length ℓ, is given by either

$$\Delta_\ell = \frac{16 \, \ell^3}{\pi^3} \sum_{n=0}^{\infty} \frac{1}{(2n+1)^2} \frac{D\Omega}{\left[(2n+1)^2 - \Omega^2 \right]^2 + D^2\Omega^2} \tag{B.3}$$

or

$$\Delta_\ell = \frac{16 \, \ell^3}{\pi^3} \frac{D\Omega}{1 + D^2\Omega^2} \tag{B.4}$$

depending on whether the exact or the approximated solution of the KGL theory is sought. The factors D and Ω have been defined such that

$$D\Omega = \frac{B\omega\ell^2}{\pi^2 C} \tag{B.5}$$

and

$$\Omega = \frac{\omega\ell}{\pi} \left(\frac{A}{C} \right)^{1/2} \quad . \tag{B.6}$$

A. Exact Solution

With substitutions from Equations (B.5) and (B.6), Equation (B.3) can be written as:

$$\Delta_\ell = \frac{16 \ B\omega}{\pi^5 C} \sum_{n=o}^{\infty} \frac{\ell^5}{(2n+1)^2} \frac{1}{\left[(2n+1)^2 - \frac{\omega^2 A \ell^2}{\pi^2 C} \right]^2 + \left(\frac{B\omega}{\pi^2 C} \right)^2 \ell^4} \qquad . \tag{B.7}$$

Rearranging terms and substituting this, along with Equation (B.2), into Equation (B.1) gives:

$$\Delta = \frac{16 \ B\omega\Lambda}{\pi^5 C} \int_0^\infty \sum_{n=o}^{\infty} \frac{\ell}{(2n+1)^2 L^2} \frac{e^{-\ell/L} \ d\ell}{\left[\frac{(2n+1)^2}{\ell^2} - \frac{\omega^2 A}{\pi^2 C} \right]^2 + \left(\frac{B\omega}{\pi^2 C} \right)^2} \qquad . \tag{B.8}$$

Introducing the change of variables, $x_n = \dfrac{\ell}{(2n+1)L}$,

$$\Delta = \frac{16 \ B\omega\Lambda}{\pi^5 C} \int_0^\infty \sum_{n=o}^{\infty} \frac{x_n e^{-(2n+1)x_n} \ dx_n}{\left[\frac{1}{L^2 x_n^2} - \frac{\omega^2 A}{\pi^2 C} \right]^2 + \left(\frac{B\omega}{\pi C} \right)^2} \qquad . \tag{B.9}$$

Considering the equation $\int f(ax) \, d(ax) = \int f(x) \, dx$, the subscript of x_n is seen to be unnecessary and is therefore dropped. Removal from the summation of terms which are independent of n leads to:

$$\Delta = \frac{16 \ B\omega\Lambda L^4}{\pi^5 C} \int_0^\infty \left[\sum_{n=o}^{\infty} e^{-(2n+1)x} \right] \frac{x^5 \ dx}{\left[1 - \frac{\omega^2 A L^2 x^2}{\pi^2 C} \right]^2 + \left(\frac{B L^2 x^2}{\pi^2 C} \right)^2} \qquad . \tag{B.10}$$

Substituting for the series, its solution

$$\sum_{n=0}^{\infty} e^{-(2n+1)x} = \frac{1}{2 \sinh (x)} \qquad \text{(B.11)}$$

gives

$$\Delta = \frac{8 B \omega \Lambda L^4}{\pi^5 C} \int_0^{\infty} \frac{x^5 \, dx}{\sinh (x) \left[\left(1 - \frac{\omega^2 A L^2 x^2}{\pi^2 C} \right)^2 + \left(\frac{B L^2 x^2}{\pi^2 C} \right)^2 \right]} \quad . \qquad \text{(B.12)}$$

Defining the constants

$$\Delta_0 = \frac{8 L^2 \Lambda}{\pi^3} \quad , \qquad \text{(B.13a)}$$

$$\omega_0 = \frac{\pi}{L} \left(\frac{C}{A} \right)^{1/2} \quad , \qquad \text{(B.13b)}$$

$$D = \frac{(B/A)}{\omega_0} \qquad \text{(B.13c)}$$

and $\qquad \Omega = \omega/\omega_0 \quad , \qquad$ (B.13d)

the net dislocation decrement can be written as:

$$\Delta = \Delta_0 \int_0^{\infty} \frac{D\Omega \, x^5 \, dx}{\sinh (x) \left[(1 - \Omega^2 x^2)^2 + D^2 \Omega^2 x^4 \right]} \quad . \qquad \text{(B.14)}$$

B. Approximate Solution

Using definition (B.5), Equation (B.4) can be written

$$\Delta_\ell = \frac{16 \; B\omega}{\pi^5 C} \; \frac{\ell^5}{1 + \left(\frac{B\omega}{\pi^2 C}\right)^2 \ell^4} \quad . \tag{B.15}$$

Substituting this and Equation (B.2) into Equation (B.1), one obtains:

$$\Delta = \frac{16 \; B\omega\Lambda}{\pi^5 C L^2} \int_0^\infty \frac{\ell^5 \; e^{-\ell/L} \; d\ell}{1 + \left(\frac{B\omega}{\pi^2 C}\right)^2 \ell^4} \quad . \tag{B.16}$$

Introducing the change of variables, $x = \ell/L$, this becomes:

$$\Delta = \frac{16 \; B\omega\Lambda L^4}{\pi^5 C} \int_0^\infty \frac{x^5 \; e^{-x} \; dx}{1 + \left(\frac{B\omega L^2}{\pi^2 C}\right)^2 x^4} \quad . \tag{B.17}$$

Using the definitions in Equations (B.13), this, the approximated net dislocation decrement, is written as

$$\Delta = 2\Delta_0 \int_0^\infty \frac{D\Omega \; x^5 \; e^{-x} \; dx}{1 + D^2\Omega^2 \; x^4} \quad . \tag{B.18}$$

VITA

Michael P. Conley was born 3 June, 1951, at Ft. Campbell, Kentucky. He graduated from Bishop Guilfoyle High School, Altoona, Pennsylvania, in June, 1969. He received his B.S. and M.S. degrees in Physics from The Pennsylvania State University in 1973 and 1975, respectively.

Mr. Conley served as a graduate teaching assistant in Physics from September, 1973 to May, 1977, and as a graduate research assistant in Physics from June, 1977 to May, 1980, at The Pennsylvania State University.

Mr. Conley is a member of the honor societies of Sigma Pi Sigma and Phi Kappa Phi.

DISTRIBUTION

FILMED

2-8